AD-F300105

AD

TECHNICAL REPORT ARBRL-TR-02432

AERODYNAMIC CHARACTERISTICS OF THE
30MM XM788E1 AND XM789 PROJECTILES

Robert L. McCoy

October 1982

DTIC
ELECTE
NOV 0 3 1982

E

US ARMY ARMAMENT RESEARCH AND DEVELOPMENT COMMAND
BALLISTIC RESEARCH LABORATORY
ABERDEEN PROVING GROUND, MARYLAND

Approved for public release; distribution unlimited.

82 10 19 021

Destroy this report when it is no longer needed.
Do not return it to the originator.

The findings in this report are not to be construed as
an official Department of the Army position, unless
so designated by other authorized documents.

REPORT DOCUMENTATION PAGE		READ INSTRUCTIONS BEFORE COMPLETING FORM
1. REPORT NUMBER Technical Report ARBRL-TR-02432	2. GOVT ACCESSION NO. AD A121 258	3. RECIPIENT'S CATALOG NUMBER
4. TITLE (and Subtitle) Aerodynamic Characteristics of the 30mm XM788E1 and XM789 Projectiles		5. TYPE OF REPORT & PERIOD COVERED Final
		6. PERFORMING ORG. REPORT NUMBER
7. AUTHOR(s) R. L. McCoy		3. CONTRACT OR GRANT NUMBER(s)
9. PERFORMING ORGANIZATION NAME AND ADDRESS U.S. Army Ballistic Research Laboratory ATTN: DRDAR-BLL Aberdeen Proving Ground, Maryland 21005		10. PROGRAM ELEMENT, PROJECT, TASK AREA & WORK UNIT NUMBERS RDT&E 1L62618AH80
11. CONTROLLING OFFICE NAME AND ADDRESS US Army Armament Research & Development Command US Army Ballistic Research Laboratory (DRDAR-BL) Aberdeen Proving Ground, Maryland 21005		12. REPORT DATE October 1982
		13. NUMBER OF PAGES 56
14. MONITORING AGENCY NAME & ADDRESS(If different from Controlling Office)		15. SECURITY CLASS. (of this report) UNCLASSIFIED
		15a. DECLASSIFICATION/DOWNGRADING SCHEDULE

16. DISTRIBUTION STATEMENT (of this Report)

Approved for public release, distribution unlimited.

17. DISTRIBUTION STATEMENT (of the abstract entered in Block 20, If different from Report)

18. SUPPLEMENTARY NOTES

19. KEY WORDS (Continue on reverse side if necessary and identify by block number)

30mm XM788E1 (TP) Projectile	Aerodynamic Drag
30mm XM789 (HEDP) Projectile	Gyroscopic Stability
Aerodynamic Characteristics	Yaw Limit-Epicycle

20. ABSTRACT (Continue on reverse side if necessary and identify by block number) (bja/ajb)

Spark range tests of the 30mm, XM788E1 (TP) and XM789 (HEDP) projectiles were conducted to determine the aerodynamic characteristics at supersonic, transonic, and subsonic speeds. Both projectiles demonstrated adequate gyroscopic stability at all speeds tested. The data show the existence of a slow arm limit-cycle yaw at high subsonic speeds, and a limit-epicycle yaw at lower subsonic speeds. The effect of the limit-epicycle on total drag is discussed.

DD FORM 1473 EDITION OF 1 NOV 65 IS OBSOLETE
1 JAN 73

TABLE OF CONTENTS

3

LIST OF ILLUSTRATIONS

LIST OF ILLUSTRATIONS (Continued)

LIST OF TABLES

I. INTRODUCTION

The first series of spark photography range tests for the 30mm, M230 Chain Gun ammunition was conducted at the Ballistic Research Laboratory (BRL) in November, 1978. At that time, only the XM788 Target Practice (TP) ammunition was available for testing, and the results of a sixteen-round firing program were reported in Reference 1. The early XM789 High-Explosive Dual-Purpose (HEDP) ammunition had experienced both in-bore mechanical failures and down-range airburst problems, and the possibility of a fuzing problem aggravated by a limit-cycle yaw at transonic and high subsonic speeds was raised as a program concern. Since no spark range tests were conducted on the early HEDP ammunition, neither the limit-cycle yaw nor the effects of moving fuze parts on the limit-cycle could be predicted. The BRL had discussed this potential problem with the office of the Project Manager for 30mm Ammunition as early as 1979, and recommended that both standard and "locked-up" fuzes should be included in the XM789 aeroballistic range tests.

In the meantime, the XM788 TP projectile had undergone design changes. The later design of the XM789 HEDP projectile body incorporated both rotating band and base section modifications, and the original TP projectile no longer looked like the re-designed HEDP. In addition, some XM788 projectiles had failed in-bore, and fragments of the broken shell bodies were observed to strike the blast suppressor. The proposed "fix" for the TP projectile consisted of changing both the shell design and the steel, and the new shell, designated the XM788E1 TP, was available for the second series of spark range tests.

The 30mm Mann barrel required for the tests was received early in 1981, as were the test authority and funds. The required ammunition components were received in April 1981, and firings were conducted in the BRL Aerodynamics Range between 24 April 1981 and 15 May 1981. The test plan called for the firing of eighteen TP rounds and eighteen HEDP rounds, distributed over a Mach number range from 2.3 down to 0.75. Four additional rounds of HEDP with "lock-up" fuzes were also fired at the lowest test velocity, to provide information on possible flight dynamic effects due to moving fuze parts.

II. TEST PROCEDURE AND MATERIAL

The 30mm projectiles, XM789 HEDP, with fuze, PD, XM759, and the XM788E1 TP are shown in the photograph of Figure 1. The "locked-up" fuze models were produced by first setting the fuze in the armed position, then "potting," or injecting epoxy resin into the fuze to solidify and lock all moving parts into a rigid structure. The "potting" added approximately 1.5 grams weight to the XM759 fuze. Figure 2 is a photograph of the cross-section of a potted fuze, and shows the cylindrical rotor aligned with the firing pin.

---

1. R. L. McCoy, "Aerodynamic Characteristics of the 30mm XM788 Projectile," Ballistic Research Laboratory Memorandum Report ARBRL-MR-03019, May 1980. AD A086096.

9

Physical measurements were taken on a sample of five TP and five HEDP rounds, and on three HEDP projectiles with potted fuzes. Figure 3 is a sketch of the XM788E1 projectile, and Figure 4 is a similar sketch for the XM789, with XM759 fuze. Average physical characteristics of the projectiles are listed in Table I.

The test rounds were fired from a 30mm Mann Barrel, Serial No. 57, designed to be an interior ballistic duplicate of the M230 Chain Gun barrel. Twist of rifling was constant, with helix angle of 6^0 30' (27.6 calibers/turn). Various propellants and charge weights were selected to achieve the required test Mach numbers. No yaw-inducer was used on any rounds in the test.

A total of twenty rounds of XM788E1 TP were successfully launched, as were nineteen XM789 HEDP rounds, and four HEDP projectiles with potted fuzes. The aerodynamic data from the forty-three successful flights are presented in this report.

III. RESULTS

The range data were fitted to solutions of the linearized equations of motion and these results used to infer linearized aerodynamic coefficients, using the methods of Reference 2. The actual projectile force-moment system often is not strictly linear, and given sufficient data, the actual non-linear behavior can be determined from the free-flight range results.[3] For the 30mm XM788E1 and XM789 projectiles, sufficient data were obtained to permit determination of some non-linear aerodynamic coefficients. A more detailed analysis of non-linear effects is presented in the various subtopics of this section which discuss individual aerodynamic coefficients.

A useful by-product of tests conducted in the BRL aerodynamics ranges is the high quality shadowgraph information obtained. Figures 5 through 14 were selected for locally small yaw (angle of attack less than 1/2 degree) and common Mach numbers, to show comparison of the flowfields around the TP and HEDP projectiles.

The round-by-round aerodynamic data for the XM788E1 TP projectile are listed in Table II, and the aerodynamic data for the XM789 HEDP are given in Table III. Free-flight motion parameters for the XM788E1 and XM789 are listed in Tables IV and V, respectively.

2. C. H. Murphy, "Data Reduction for the Free Flight Spark Ranges," Ballistic Research Laboratories Report No. 900, February 1954. AD 35833.

3. C. H. Murphy, "The Measurement of Non-Linear Forces and Moments by Means of Free Flight Tests," Ballistic Research Laboratories Report No. 974, February 1956. AD 93521.

A. Drag Coefficient

The drag coefficient, C_D, is determined by fitting the time-distance measurements from the range flight. C_D is distinctly non-linear with yaw level, and the value determined from an individual flight reflects both the zero-yaw drag coefficient, C_{D_0}, and the induced drag due to the average yaw level of the flight. The drag coefficient variation is expressed as an even power series in yaw amplitude:

$$C_D = C_{D_0} + C_{D_{\delta^2}} \delta^2 + \ldots\ldots$$

(1)

where C_{D_0} is the zero-yaw drag coefficient, $C_{D_{\delta^2}}$ is the quadratic yaw-drag coefficient, and δ^2 is the total angle of attack squared.

Analysis of the drag coefficient data for the two 30mm projectiles showed that the zero-yaw drag coefficients were, for practical purposes, identical. However, the yaw-drag coefficient for the TP projectile was found to be significantly higher than that for the HEDP design, at both supersonic and subsonic speeds.

The yaw-drag coefficients obtained from the analysis were used to correct the range values of C_D to zero-yaw conditions. Figures 15 and 16 show the variation of C_{D_0} with Mach number for the XM788E1 TP and the XM789 HEDP shell respectively. Figure 17 shows the behavior of the yaw-drag coefficients for the two projectiles. Although the $C_{D_{\delta^2}}$ curves are significantly different, the resulting total in-flight drag values, for the expected average yaw levels, differ by less than 2% at supersonic speeds, and less than 4% at subsonic speeds. The TP round will experience slightly higher total drag at all speeds than will the HEDP round.

B. Pitching Moment Coefficient

The range values of the pitching moment coefficient, C_{M_α}, were fitted using the appropriate squared-yaw parameters from Reference 3. C_{M_α} was found to vary significantly with yaw level for the 30mm projectiles. The pitching moment is assumed to be cubic in yaw level, and the coefficient variation is given by:

$$C_{M_\alpha} = C_{M_{\alpha_0}} + C_2 \delta^2$$

(2)

11

where $C_{M_{\alpha_0}}$ is the zero-yaw pitching moment coefficient, and C_2 is the cubic coefficient.

For both the TP and HEDP projectiles, the value of C_2 at supersonic speeds was found to -14; the corresponding value at subsonic and transonic speeds was -8. These values were used to correct the range values of C_{M_α} to zero-yaw conditions. Figures 18 and 19 show the variation of $C_{M_{\alpha_0}}$ with Mach number for the TP and HEDP shell, respectively. The TP round shows approximately 3% higher pitching moment than the HEDP round at subsonic and transonic speeds; at high supersonic speeds the curves for the two shells are practically identical. Note that the $C_{M_{\alpha_0}}$ for the potted fuze rounds is about 3% lower than that of standard HEDP shell at $M_\infty = 0.75$. This effect reflects the forward shift in center of gravity location caused by adding 1.5 grams of potting resin into the fuze.

C. Gyroscope Stability

The 30mm, XM788E1 TP and XM789 HEDP projectiles have ample launch gyroscope stability when fired at standard velocity (805 metres/second) from the 6° 30' twist rate (27.6 calibers/turn) of the M230 barrel. The average launch gyroscopic stability factor (Sg) of both projectiles at standard atmospheric conditions is 3.0. Since neither projectile will ever be fired at reduced velocities, and the ratio of axial spin to forward velocity increases continuously for flat trajectories, the slightly lower values of S_g observed in Tables IV and V for the lower Mach numbers will never occur in field firings.

The 30mm projectiles are designed to be launched in forward fire from an aircraft. The addition of the aircraft's velocity vector to the gun muzzle velocity has the effect of reducing the projectile's launch gyroscopic stability factor by the ratio:

$$\left(\frac{V_{Muzzle}}{V_{A/C} + V_{Muzzle}} \right)^2$$

where $V_{A/C}$ is the forward velocity of the aircraft.

The following table shows the effect of aircraft speed on launch Sg, for both TP and HEDP ammunition in foward fire.

$V_{A/C}$	S_g
(Knots)	(Launch)
0	3.00
150	2.50
300	2.11
450	1.80
550	1.64

At an aircraft speed of 550 knots, the M230 Chain Gun ammunition still has more than adequate gyroscopic stability.

D. Lift Force Coefficient

The lift force coefficient, C_{L_α}, was also analyzed by the method of Reference 3. If the lift force is assumed to be cubic in yaw level, the coefficient variation is given by:

$$C_{L_\alpha} = C_{L_{\alpha_0}} + a_2 \, \delta^2$$

(3)

where $C_{L_{\alpha_0}}$ is the zero-yaw lift force coefficient, and a_2 is the cubic coefficient.

No significant value of the cubic lift coefficient could be found, for either projectile tested, at any speed. Further analysis showed that no significant difference existed in the range values of C_{L_α}, between the TP and the HEDP shell. Figure 20 shows the variation of C_{L_α} with Mach number for the two projectiles.

The lift force coefficient is not as well determined from spark range tests as is the pitching moment coefficient. This fact is reflected in the larger round-to-round data scatter observed in Figure 20, compared with the pitching moment data plotted in Figures 18 and 19.

E. Magnus Moment Coefficient and Pitch Damping Moment Coefficient

The Magnus moment coefficient, $C_{M_{p\alpha}}$, and the Pitch Damping Moment Coefficient, $\left(C_{M_q} + C_{M_{\dot{\alpha}}}\right)$, are discussed together, since if either coefficient is non-linear with yaw level, both coefficients exhibit non-linear coupling in the data reduction process[3]. Due to mutual reaction, the analysis of

13

$C_{M_{p\alpha}}$ and $\left(C_{M_q} + C_{M_{\dot\alpha}}\right)$ must be performed simultaneously, although the aerodynamic moments are not, in themselves, directly physically related.

If the dependence of both the Magnus moment and the Pitch Damping moment are cubic in yaw level, the non-linear variation of the two moment coefficients is of the general form:

$$C_{M_{p\alpha}} = C_{M_{p\alpha_0}} + \hat{C}_2 \delta^2 \tag{4}$$

$$\left(C_{M_q} + C_{M_{\dot\alpha}}\right) = \left(C_{M_q} + C_{M_{\dot\alpha}}\right)_0 + d_2 \delta^2 \tag{5}$$

where $C_{M_{p\alpha_0}}$ and $\left(C_{M_q} + C_{M_{\dot\alpha}}\right)_0$ are the zero-yaw values of Magnus and Pitch Damping moment coefficients, respectively, and $\hat{C}_2$ and d_2 are the associated cubic coefficients.

In Reference 3 it is shown that the non-linear coupling introduced through the data reduction yields the following expressions for range values [R-subscript] of $C_{M_{p\alpha}}$ and $\left(C_{M_q} + C_{M_{\dot\alpha}}\right)$:

$$\left[C_{M_{p\alpha}}\right]_R = C_{M_{p\alpha_0}} + \hat{C}_2 \delta_e^2 + d_2 \delta_{e_{TH}}^2 \tag{6}$$

$$\left[C_{M_q} + C_{M_{\dot\alpha}}\right]_R = \left(C_{M_q} + C_{M_{\dot\alpha}}\right)_0 + \hat{C}_2 \delta_{e_{HT}}^2 + d_2 \delta_{e_{HH}}^2 \tag{7}$$

where the above effective squared yaws are defined as:

$$\delta_e^2 = K_F^2 + K_S^2 + \left(\phi_F' K_F^2 - \phi_S' K_S^2\right) \Big/ \left(\phi_F' - \phi_S'\right) \tag{8}$$

$$\delta_{e_{TH}}^2 = \left(I_x/I_y\right) \left[\left(K_F^2 \phi_F'^2 - K_S^2 \phi_S'^2\right) \Big/ \left(\phi_F'^2 - \phi_S'^2\right)\right] \tag{9}$$

$$\delta_{e_{HT}}^2 = \left(I_y/I_x\right) \left(\phi_F' + \phi_S'\right)\left(K_S^2 - K_F^2\right) \Big/ \left(\phi_F' - \phi_S'\right) \tag{10}$$

14

$$\delta_{e_{HH}}{}^2 = \left(\phi_F' K_S{}^2 - \phi_S' K_F{}^2\right)\Big/\left(\phi_F' - \phi_S'\right) \tag{11}$$

The remaining symbols are defined in the List of Symbols in this report.

Preliminary analysis of the XM788E1 and XM789 data showed no significant non-linearity in either $C_{M_{p\alpha}}$ or $C_{M_q} + C_{M_{\dot\alpha}}$, at supersonic speeds. However, at transonic and subsonic speeds, the two coefficients showed strong non-linear coupling, and it was necessary to perform the analysis on both coefficients simultaneously.

The data rounds were first separated into Mach number groups, by round type, and individual values of the two cubic coefficients were obtained. Next, a statistical analysis was performed, which yielded the useful result that there was no significant difference between the TP and HEDP rounds, in either linear or cubic coefficients. The further result that the potted fuze rounds were statistically the same population as standard HEDP rounds completed the preliminary analysis, and all round types were then combined for final analysis.

The combined data rounds were again separated into Mach number groups, and final values of the cubic coefficients were obtained at five average Mach numbers through the transonic-subsonic range. The values of $\hat{C}_2$ and d_2 fell nearly along straight lines, and a weighted linear least squares fit of the cubic coefficients was used to correct the range values $C_{M_{p\alpha}}$ and $C_{M_q} + C_{M_{\dot\alpha}}$ to zero-yaw conditions. Figures 21 and 22 show the variation of $C_{M_{p\alpha_0}}$ and $\left(C_{M_q} + C_{M_{\dot\alpha}}\right)_0$, respectively, with Mach number. Figures 23 and 24 show the variation of the cubic Magnus moment coefficient, $\hat{C}_2$, and the cubic pitch-damping moment coefficient, d_2, with Mach number. Figures 21 and 22 include individual round coefficients, corrected to zero-yaw values, and visually confirm the fact that no significant differences in Magnus or pitch-damping moments exist between the TP and HEDP rounds. The same two figures also imply that no significant flight dynamic difference should be observed between standard and "locked-up" XM759 fuzes, with the HEDP shell.

F.   Flight Dynamic Predictions

The damping rates, λ_F and λ_S, of the fast and slow yaw modes indicate the dynamic stability of a projectile. Negative λ's indicate damping; a positive λ means that its associated modal arm will grow with increasing time.

15

For a projectile whose Magnus or pitch-damping moments are non-linear with yaw level, the damping rates also show a non-linear dependence on yaw. In Reference 4, Murphy successfully predicted the effect of a cubic Magnus moment on the damping rates by means of an amplitude-plane analysis. However, the amplitude-plane technique becomes cumbersome for a projectile with both Magnus and pitch-damping moment non-linearities. The effects of changing epicyclic frequencies along the trajectory, in addition to variations in the values of aerodynamic coefficients with Mach number further increase the difficulty in application of the amplitude-plane method to long-range flight dynamic problems.

For purposes of this report, the BRL six-degree-of-freedom (6-DOF) trajectory program[5] was used to predict the long range flight dynamic performance of XM788E1 and XM789 ammunition. The 6-DOF program results for the prototype XM788 projectile had previously been compared with numerical integration of the damping rate equations[1], and the agreement between the two methods was very close. Since the 6-DOF trajectory program includes all the effects of changing axial spin and aerodynamic coefficient variations with Mach number, it represents the best approximation to real-range flight dynamic prediction.

The 6-DOF trajectory program was run for an XM789 HEDP projectile launched at a muzzle velocity of 805 metres/second, and with an initial yaw rate of 20 radians/second, which produces a first maximum yaw of about 2-1/2 degrees. Analysis of the trajectory program output shows the fast arm damped to an insignificant level at 1,000 metres range, where the flight Mach number is approximately one; the slow arm at the same range has damped to around 0.1 degree in amplitude. The above situation persists until approximately 1,300 metres range ($M_\infty = 0.85$), where the slow arm amplitude begins to grow. At 1,500 metres range ($M_\infty = 0.77$), the slow arm has grown to a local maximum value of about 2.1 degrees, and at this point the fast arm, which had remained very small since the low supersonic region, begins to grow. The fast arm amplitude attains a maximum value of approximately 1.6 degrees at about 1,750 metres range ($M_\infty = 0.69$). Thus, the dynamic performance of the XM789 shell at subsonic speeds is described as a "limit-epicycle," rather than the slow arm limit-cycle motion previously observed[1] for the XM788 projectile. Figure 25 shows the predicted variation of the fast and slow arm amplitudes with Mach number for the XM789 shell. A similar trajectory was run for the XM788E1, with substantially identical results.

The dashed curves shown in Figure 25 must be considered as estimated trends, because they are based on extrapolated aerodynamic data. No firings were conducted in the BRL Aerodynamics Range below Mach number 0.70, due to high gravity-induced trajectory curvature at low velocities. For the 6-DOF

4. C. H. Murphy, "Free Flight Motion of Symmetric Missiles," Ballistic Research Laboratories Report No. 1216, July 1963. AD 442757.

5. R. F. Lieske and R. L. McCoy, "Equations of Motion of a Rigid Projectile," Ballistic Research Laboratories Report No. 1244, March 1964. AD 441598.

trajectory simulations, all aerodynamic coefficients were assumed constant below Mach number 0.7, and the spin damping moment coefficient, C_{l_p}, from Reference 1 was used for simulations of the current 30mm projectiles. Since the presently available aerodynamic data has "run out" at a real range of approximately 1,750 metres, and the intended use of the 30mm gun system envisions firing to ranges of three kilometers and beyond, it is highly recommended that a long-range instrumented flight dynamic test similar to that recommended in Reference 1, be conducted for the XM788E1 and XM789 shell, to verify the estimated trends of this report.

The spin damping moment coefficient, C_{l_p}, was not measured for the XM788E1 and XM789 projectiles. The spin damping data previously obtained for the XM788 TP shell are considered sufficiently accurate to describe the spin performance of the current projectiles, and the C_{l_p} curve presented in Reference 1 is reproduced in this report as Figure 26.

IV. CONCLUSIONS

The 30mm, XM788E1 TP and XM789 HEDP projectiles, when launched at a muzzle velocity of 805 metres/second from the M230 barrel, are gyroscopically stable in either forward or side fire, from aircraft at speeds up to 550 knots.

The spark range data predict that a limit-epicycle yaw exists for both shell at subsonic speeds. The predicted slow arm amplitude is approximately two degrees, and the fast arm amplitude is around one and one-half degrees. The limit-epicycle yaw will produce drag increases of between four and eight percent over the zero-yaw values at subsonic speeds.

V. RECOMMENDATIONS

It is recommended that a long-range flight dynamic experiment be conducted to verify the predicted subsonic limit-epicycle behavior of the XM788E1 and XM789 projectiles. The flight dynamic tests should be conducted using the M230 Chain Gun, and the flight dynamic information could best be obtained using the 30mm yawsonde fuze currently under development at the BRL.

We have recently been advised that the M230 Chain Gun barrel has been changed from the constant-twist rifling used in the present tests to a gain-twist form of rifling. It is recommended that a limited re-test of XM788E1 and XM789 ammunition be conducted from the new barrel, at standard muzzle velocity, to insure validity of the present aerodynamic data for rounds with a different engraving pattern on the rotating bands.

17

Table I. Average Physical Characteristics of 30mm Projectiles

Projectile	Reference Diameter (mm)	Weight (grams)	Center of Gravity (calibers, base)	Axial Moment of Inertia (gm-cm²)	Transverse Moment of Inertia (gm-cm²)
XM788E1 (TP)	29.92	239.0	1.35	330.2	1743
XM789 (HEDP)	29.92	234.6	1.40	313.6	1619
XM789, with Potted Fuze	29.92	236.1	1.41	313.7	1640

Table II. Aerodynamic Coefficients of the 30mm, XM788E1 TP Projectile

Rd. No.	Mach Number	α_t (deg)	C_D	C_{M_α}	C_{L_α}	$C_{M_{P\alpha}}$	$(C_{M_q} + C_{M_{\dot\alpha}})$	CP_N (cal-base)
14725	2.307	.99	.4120	2.39	2.51	.12	-4.19	2.17
14718	2.290	1.55	.4132	2.35	2.53	.00	-4.22	2.15
14716	2.284	.79	.4161	2.39	2.23	---	---	2.25
14724	2.271	.52	.4093	2.34	2.56	---	---	2.14
14717	2.263	.95	.4149	2.37	2.29	---	---	2.23
14726	1.811	.69	.4525	2.65	2.31	---	---	2.31
14727	1.768	1.70	.4730	2.59	2.51	-.09	-5.13	2.22
14732	1.274	1.19	.5202	2.80	2.38	---	---	2.31
14731	1.258	1.21	.5320	2.83	2.81	---	---	2.20
14739	.995	1.04	.4022	2.96	1.74	---	---	2.73
14737	.994	1.74	.4143	2.99	1.55	-.98	4.92	2.87
14738	.993	1.21	.4085	3.13	2.54	---	---	2.41
14736	.990	2.83	.4140	2.98	2.28	-.56	.53	2.45
14743	.922	1.99	.2727	2.94	1.89	-.62	3.16	2.71
14744	.891	3.11	.2690	2.77	2.00	-.36	.86	2.57
14742	.866	.81	.2468	2.81	2.54	---	---	2.36
14748	.758	1.89	.2530	2.71	2.23	-.81	6.30	2.44
14752	.743	.92	.2400	2.54	2.22	---	---	2.38
14749	.741	.91	.2403	----	----	---	---	---
14751	.725	1.78	.2401	2.60	1.90	-1.19	10.53	2.57

Table III. Aerodynamic Coefficients of the 30mm, XM789 HEDP Projectile

Rd. No.	Mach Number	α_t (deg)	C_D	C_{M_α}	C_{L_α}	$C_{M_{P\alpha}}$	$(C_{M_q} + C_{M_{\dot\alpha}})$	CP_N (cal-base)
14721	2.264	.45	.4059	2.28	2.25	---	---	2.26
14723	2.262	.57	.4098	2.36	2.15	---	---	2.32
14722	2.262	.12	.4125	---	---	---	---	---
14720	2.254	1.16	.4071	2.33	2.51	.05	-4.84	2.20
14719	2.234	.75	.4086	2.37	2.34	---	---	2.26
14728	1.826	.59	.4563	2.60	3.05	---	---	2.14
14729	1.782	1.73	.4655	2.58	2.57	-.01	-4.52	2.25
14734	1.278	2.03	.5365	2.74	2.19	-.09	-3.69	2.41
14733	1.277	1.44	.5197	2.62	2.42	---	---	2.30
14740	.992	1.71	.4142	2.84	---	-.64	2.73	---
14741	.989	.99	.4081	2.91	2.13	---	---	2.55
14746	.899	2.59	.2627	2.72	2.09	-.86	5.11	2.56
14747	.880	1.19	.2437	2.71	1.55	---	---	2.92
14745	.872	2.08	.2508	2.74	1.89	-.69	5.23	2.68
14756	.761	2.03	.2477	2.58	2.15	-.93	8.49	2.48
14754	.761	1.54	.2430	2.46	2.58	---	---	2.28
14753	.760	1.78	.2416	2.55	2.06	-.88	8.95	2.50
14755	.749	2.40	.2450	2.57	1.90	-.68	5.37	2.60
14750	.737	1.79	.2404	2.58	1.93	-.39	7.17	2.59
*14760	.764	2.64	.2445	2.38	2.13	-.94	4.78	2.41
*14758	.741	1.91	.2463	2.49	2.16	-.55	4.58	2.45
*14757	.725	2.13	.2401	2.41	2.30	-1.70	11.31	2.36
*14759	.723	2.07	.2379	2.46	1.85	-1.15	10.33	2.59

*Potted Fuze Round

20

Table IV.   Flight Motion Parameters of the 30mm, XM788E1 TP Projectile

Rd. No.	Mach Number	S_g	S_d	$\lambda_F \times 10^3$ (1/cal)	$\lambda_S \times 10^3$ (1/cal)	K_F	K_S	ϕ'_F (rad/cal)	ϕ'_S (rad/cal)
14725	2.307	3.13	.87	-.231	-.172	.0118	.0135	.0402	.0039
14718	2.290	3.18	.67	-.288	-.131	.0158	.0208	.3405	.0038
14716	2.284	3.13	---	----	----	.0081	.0109	.0400	.0038
14724	2.271	3.20	---	----	----	.0041	.0074	.0405	.0038
14717	2.263	3.15	---	----	----	.0091	.0128	.0405	.0038
14726	1.811	2.86	---	----	----	.0069	.0096	.0399	.0043
14727	1.768	2.96	.44	-.385	-.080	.0158	.0221	.0401	.0041
14732	1.274	2.81	---	----	----	.0126	.0159	.0410	.0045
14731	1.258	2.75	---	----	----	.0111	.0169	.0407	.0046
14739	.995	2.52	---	----	----	.0110	.0143	.0391	.0049
14737	.994	2.47	---	-.049	.315	.0226	.0200	.0388	.0050
14738	.993	2.41	---	----	----	.0153	.0146	.0389	.0052
14736	.990	2.49	-1.73	-.185	.092	.0309	.0383	.0390	.0050
14743	.922	2.46	---	-.009	.137	.0247	.0243	.0387	.0050
14744	.891	2.54	-.75	-.076	.023	.0377	.0390	.0384	.0048
14742	.866	2.57	---	----	----	.0072	.0109	.0387	.0048
14748	.758	2.68	---	.135	.158	.0248	.0213	.0391	.0045
14752	.743	2.89	---	----	----	.0083	.0116	.0394	.0042
14749	.741	---	---	.583	.197	.0137	.0066	.G397	.0050
14751	.725	2.79	---	.295	.307	.0192	.0239	.0393	.0043

21

Table V. Flight Motion Parameters of the 30mm, XM789 HEDP Projectile

Rd. No.	Mach Number	S_g	S_d	$\lambda_F \times 10^3$ (1/cal)	$\lambda_S \times 10^3$ (1/cal)	K_F	K_S	ϕ'_F (rad/cal)	ϕ'_S (rad/cal)
14721	2.264	3.24	---	---	---	.0050	.0053	.0418	.0039
14723	2.262	3.12	---	---	---	.0054	.0079	.0416	.0040
14722	2.262	---	---	---	---	.0013	.0017	.0418	.0054
14720	2.254	3.19	.66	-.345	-.143	.0117	.0154	.0419	.0039
14719	2.234	3.15	---	---	---	.0063	.0109	.0419	.0040
14728	1.826	2.91	---	---	---	.0069	.0076	.0416	.0044
14729	1.782	3.03	.60	-.345	-.119	.0187	.0219	.0425	.0042
14734	1.278	2.89	.46	-.321	-.070	.0202	.0278	.0427	.0045
14733	1.277	2.68	---	---	---	.0111	.0211	.0399	.0046
14740	.992	2.50	---	-.063	.183	.0211	.0211	.0397	.0051
14741	.989	2.50	---	---	---	.0079	.0143	.0403	.0051
14746	.899	2.52	---	.028	.218	.0305	.0332	.0392	.0049
14747	.880	2.57	---	---	---	.0112	.0159	.0396	.0049
14745	.872	2.59	---	.131	.144	.0279	.0233	.0401	.0049
14756	.761	2.84	---	.260	.226	.0267	.0222	.0406	.0044
14754	.761	2.87	---	---	---	.0124	.0212	.0400	.0043
14753	.760	2.85	---	.316	.190	.0218	.0213	.0406	.0044
14755	.749	2.83	---	.124	.142	.0284	.0304	.0407	.0044
14750	.737	2.82	---	.412	.001	.0234	.0202	.0409	.0045
*14760	.764	2.86	---	-.031	.253	.0260	.0374	.0392	.0042
*14758	.741	2.85	---	.119	.055	.0269	.0194	.0396	.0043
*14757	.725	2.89	---	.134	.507	.0222	.0279	.0394	.0042
*14759	.723	2.87	---	.300	.306	.0238	.0259	.0397	.0042

*Potted Fuze Round

22

XM789

HEDP

XM788E1

TP
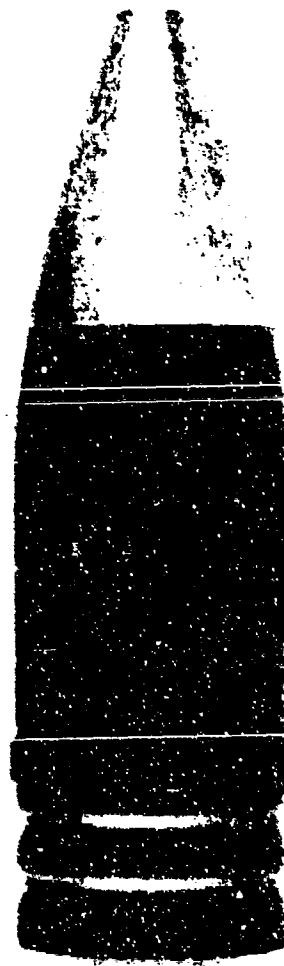
Figure 1. Photograph of 30mm XM789 and XM788E1 Projectiles.
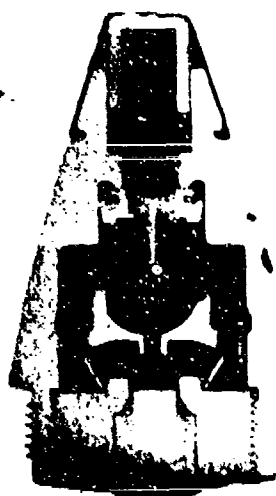
Figure 2.   Photograph of the Cross Section of "Potted" XM759 Fuze.
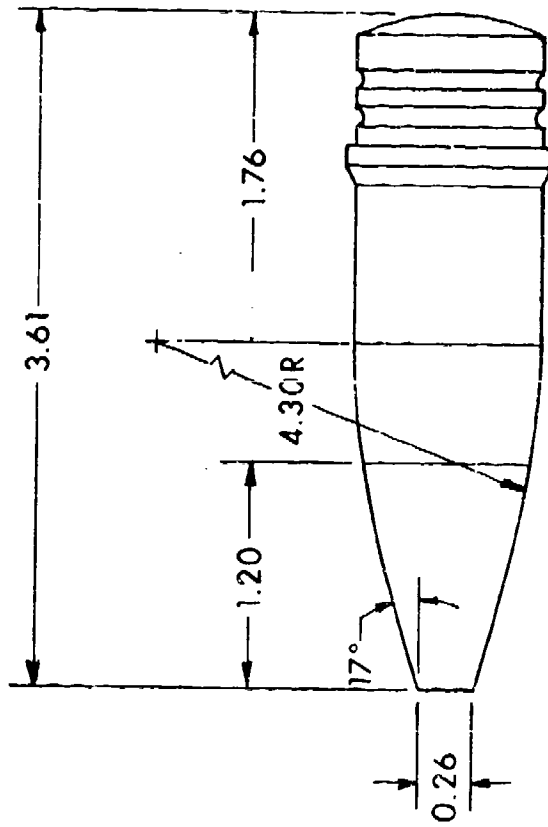
ALL DIMENSIONS IN CALIBERS
(1 CALIBER = 29.92 mm)

Figure 3. Sketch of 30mm, XM788E1 TP Projectile

25
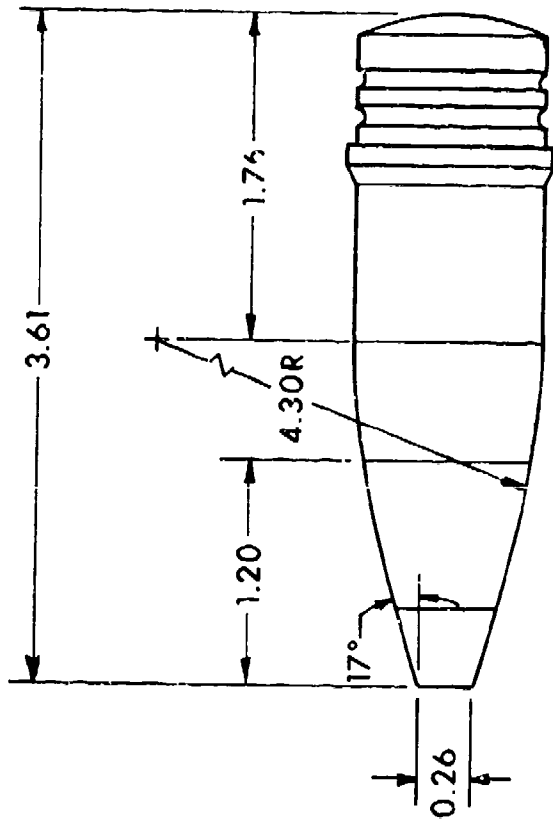
ALL DIMENSIONS IN CALIBERS
(1 CALIBER = 29.92 mm)

Figure 4.   Sketch of 30mm, XM789 HEDP Projectile
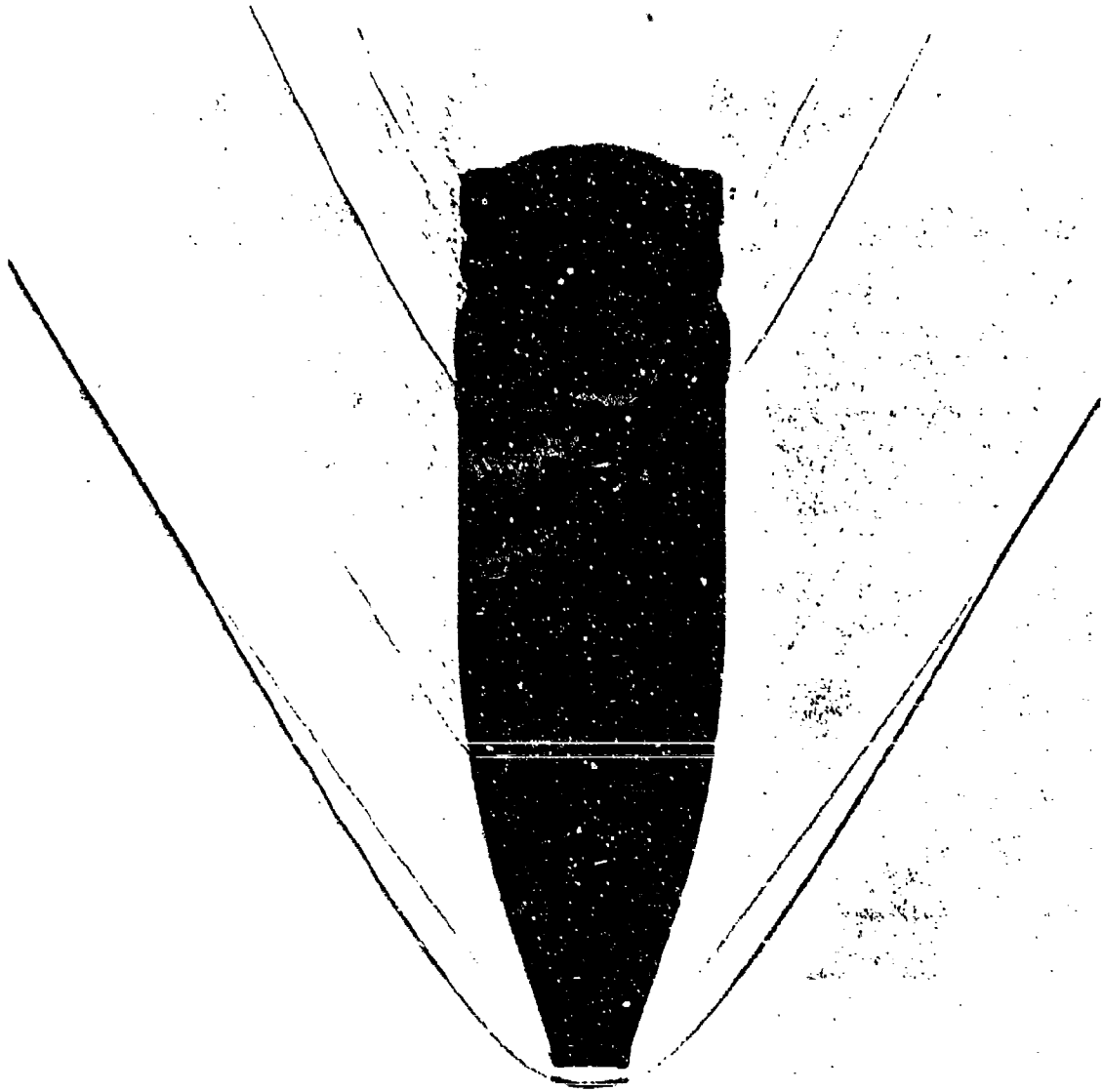
Figure 5. Shadowgraph of TP Projectile at Mach 2.30.
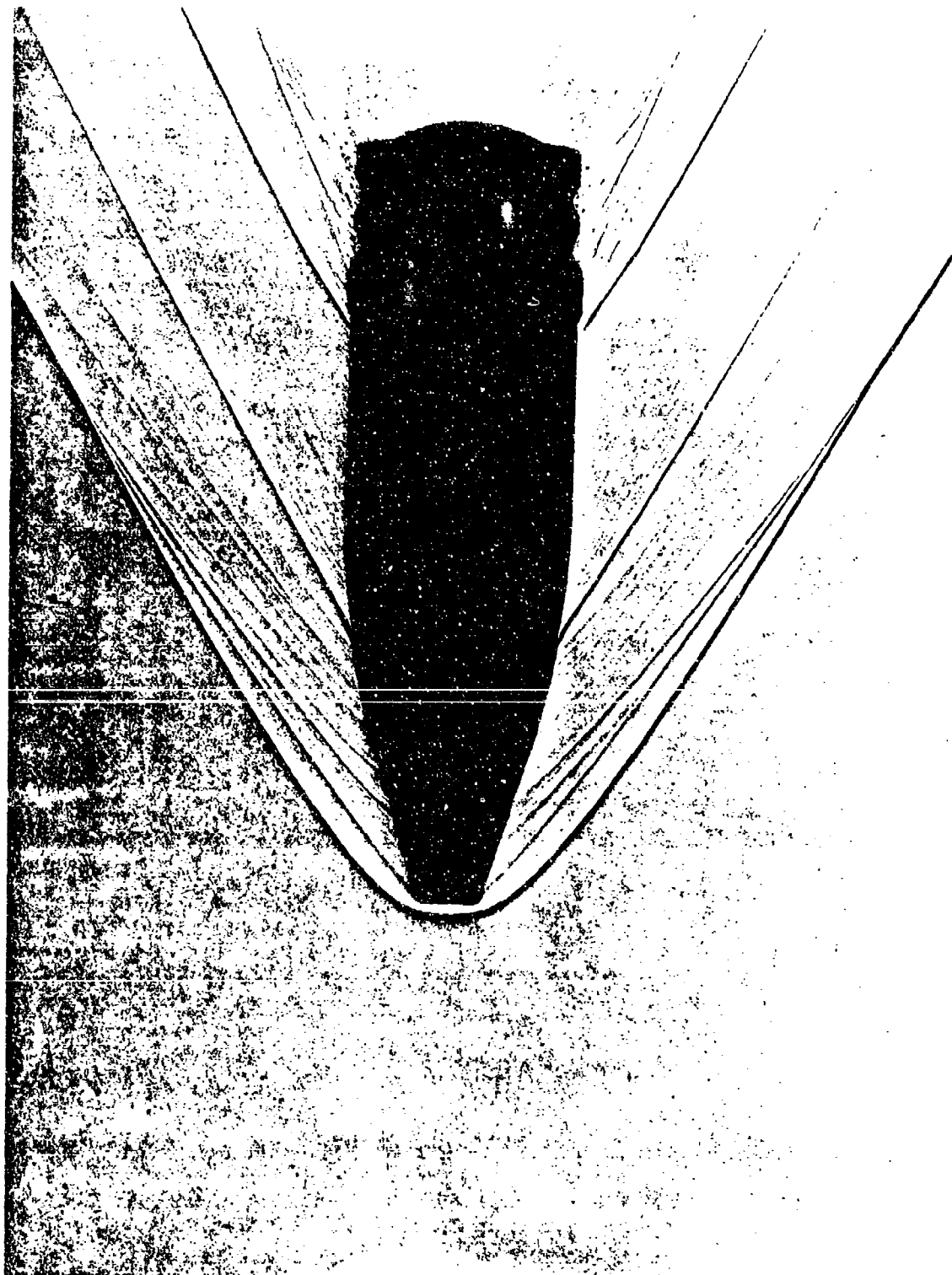
Figure 6. Shadowgraph of HEDP Projectile at Mach 2.30.

28
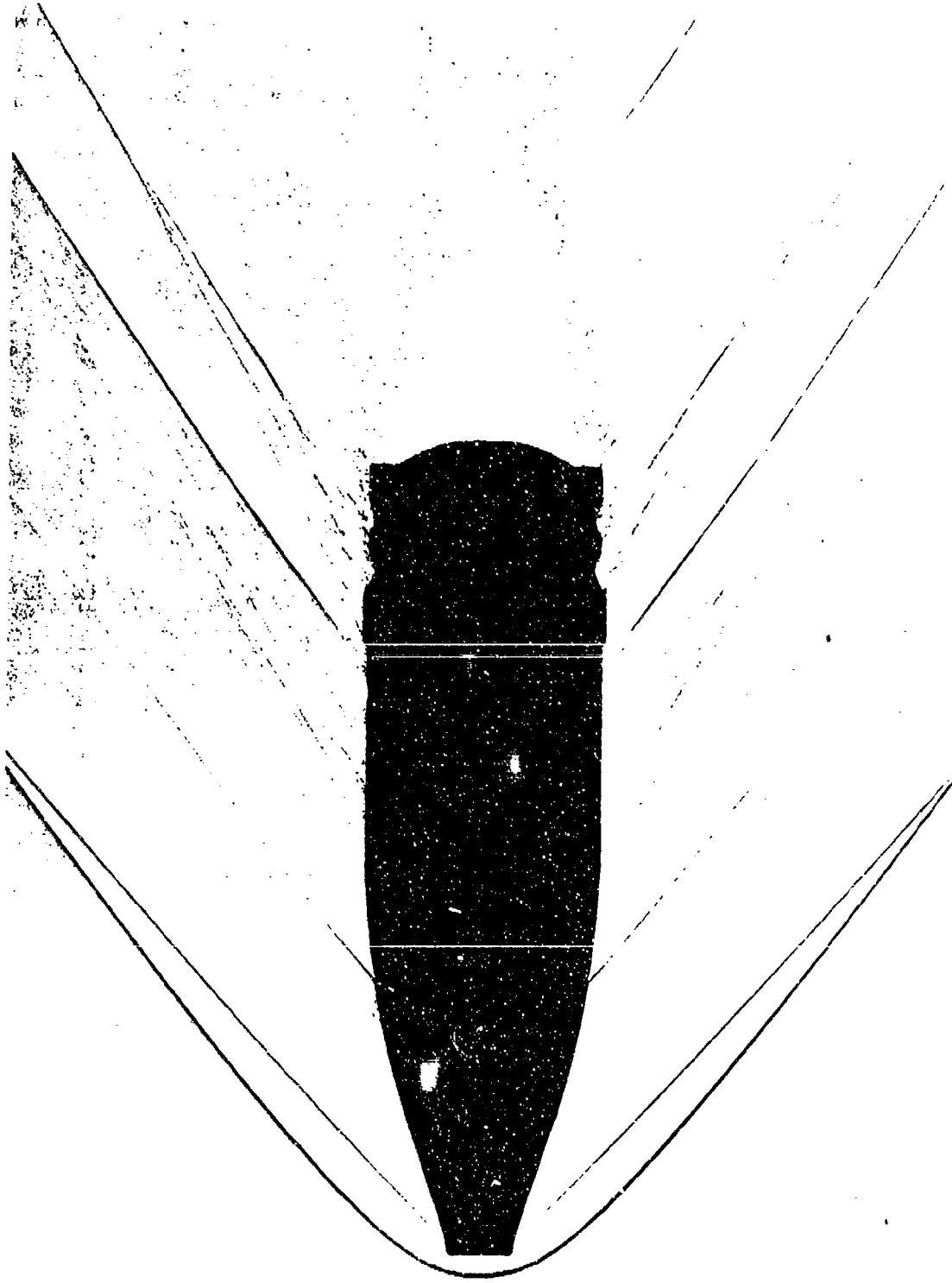
Figure 7. Shadowgraph of TP Projectile at Mach 1.85.
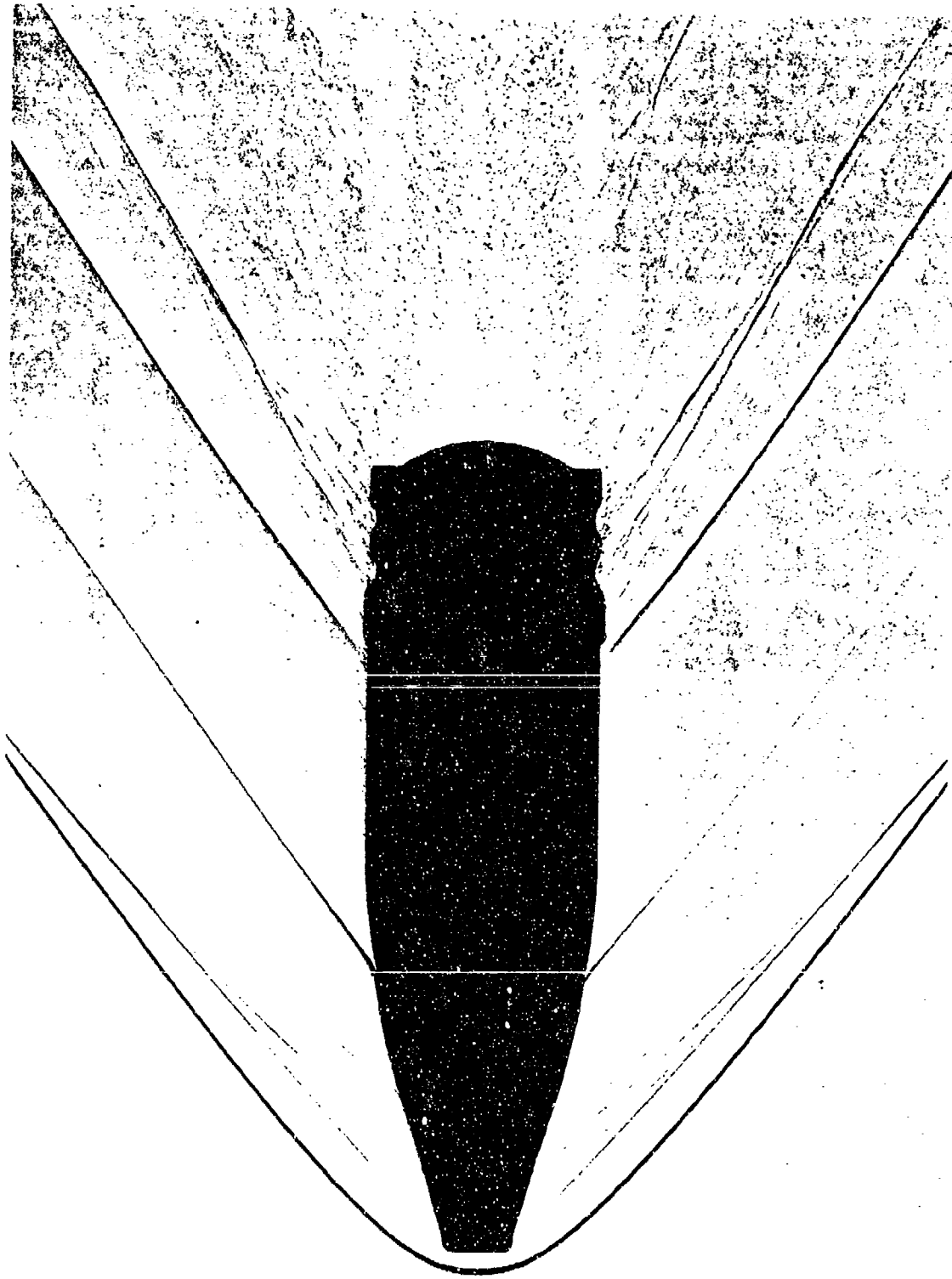
Figure 8. Shadowgraph of HEDP Projectile at Mach 1.85.
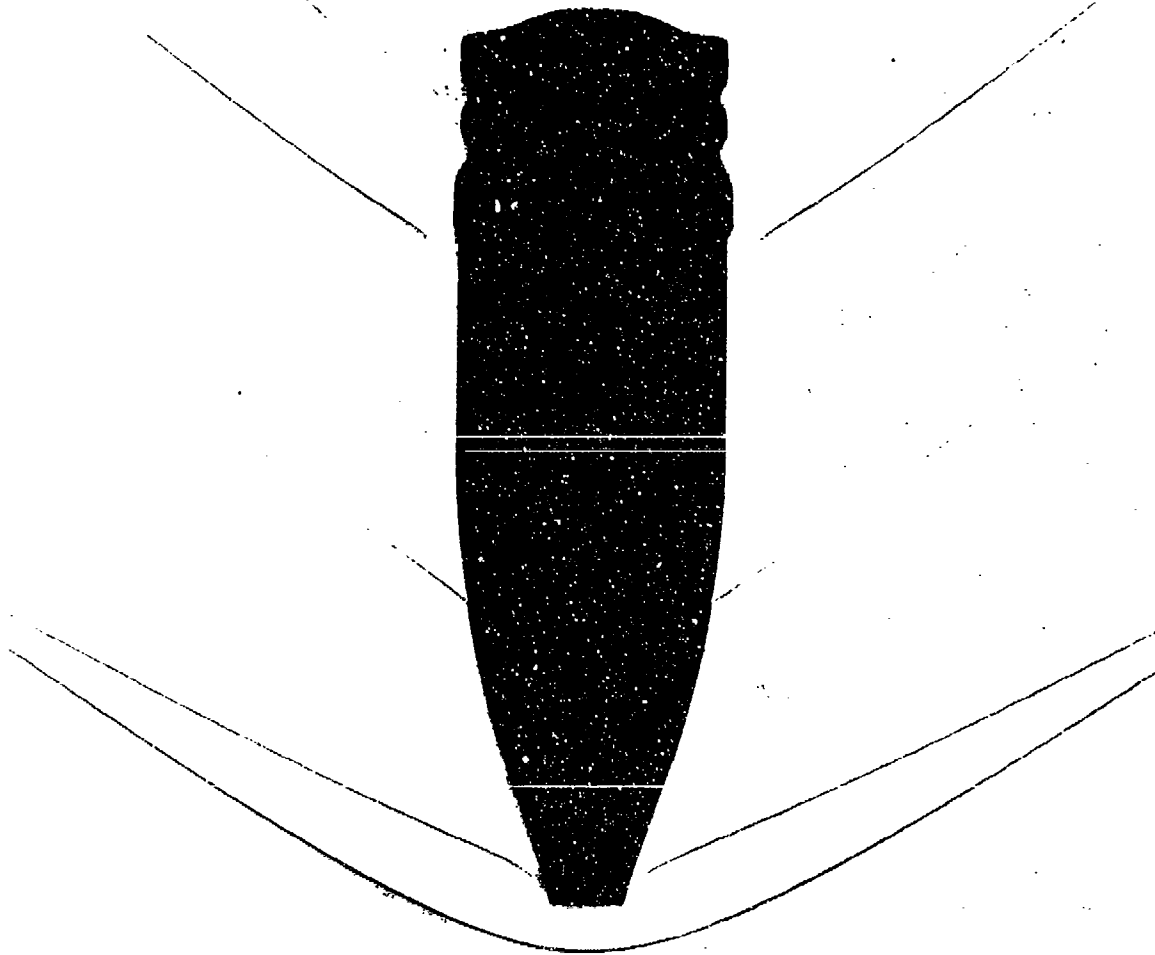
Figure 9. Shadowgraph of TP Projectile at Mach 1.30.
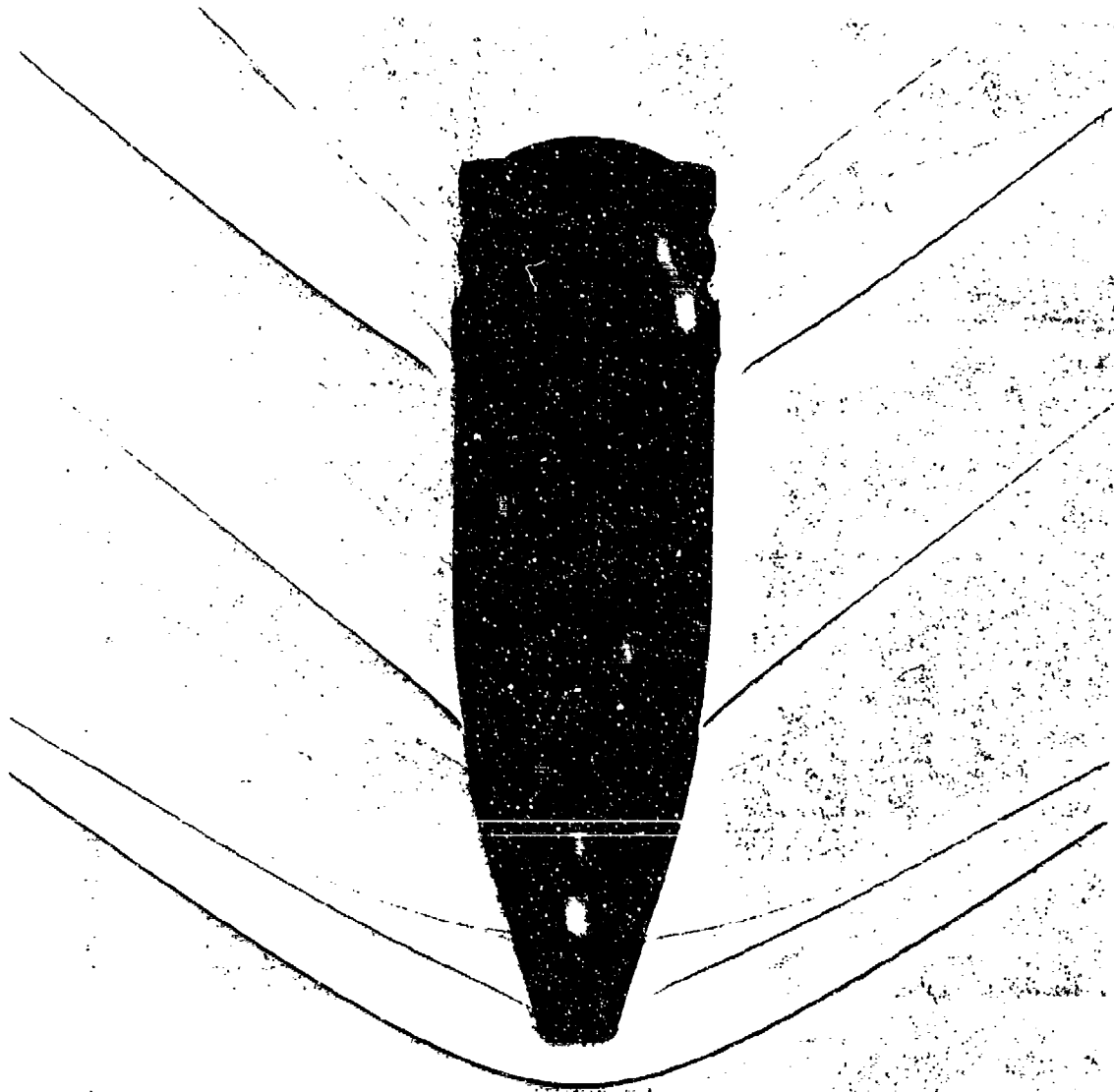
Figure 10. Shadowgraph of HEDP Projectile at Mach 1.30.
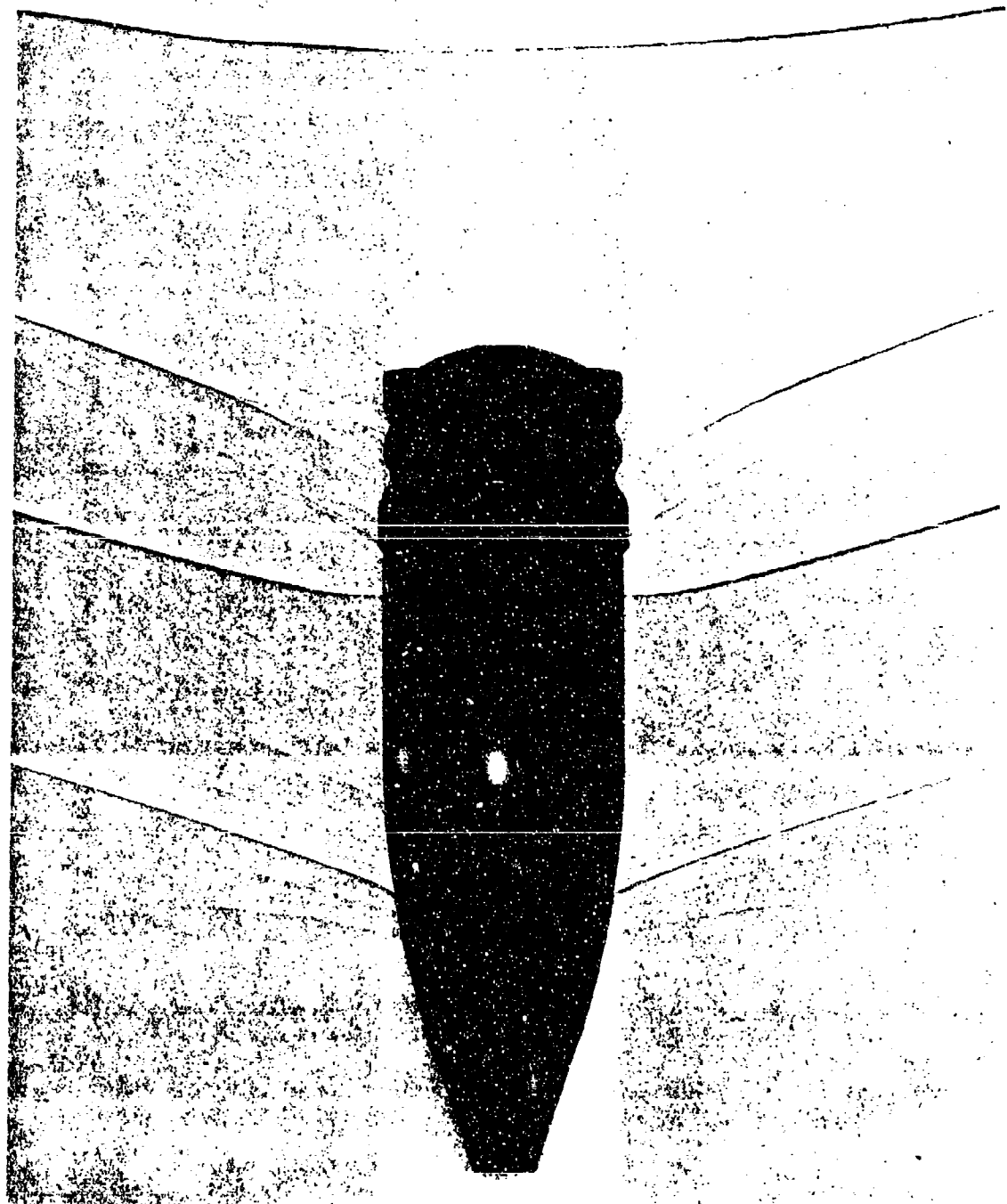
Figure 11. Shadowgraph of TP Projectile at Mach 1.00.
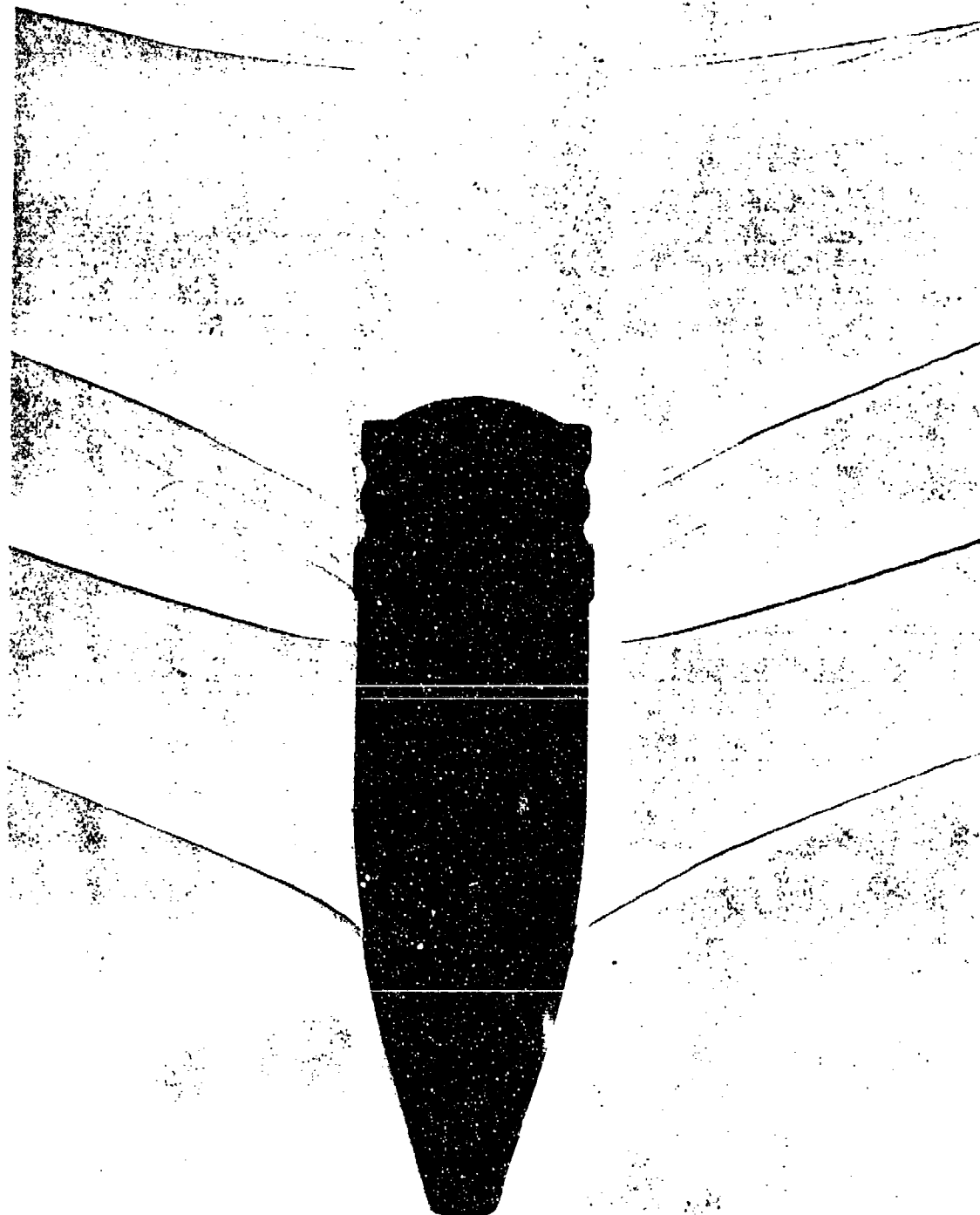
Figure 12. Shadowgraph of HEDP Projectile at Mach 1.00.
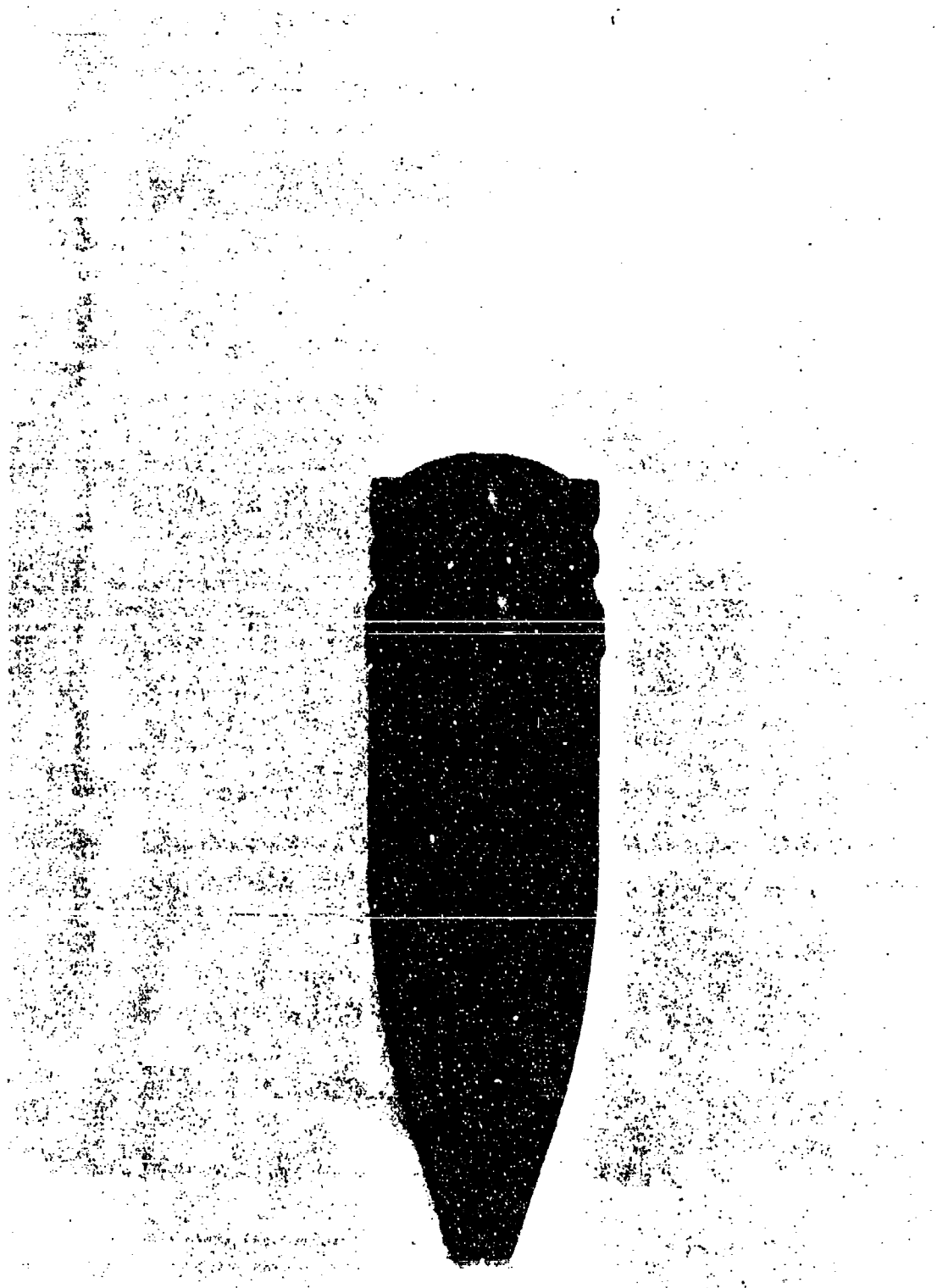
Figure 13. Shadowgraph of TP Projectile at Mach 0.74.

Figure 14. Shadowgraph of HEDP Projectile at Mach 0.74.
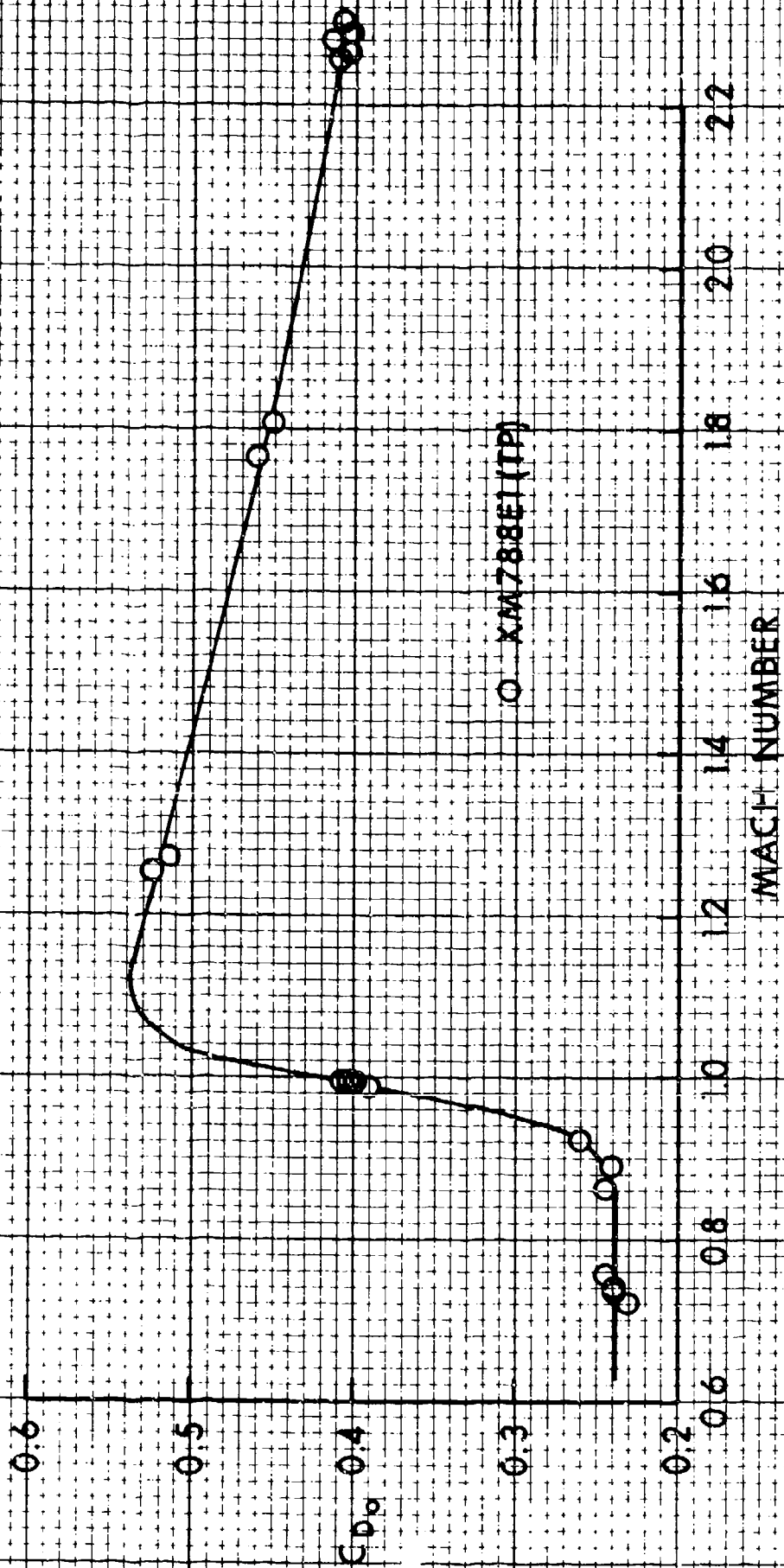
Figure 15. Zero-Yaw Drag Force Coefficient versus Mach Number, XM788E1

○ XM788E1(TP)

MACH NUMBER

C_{D_O}
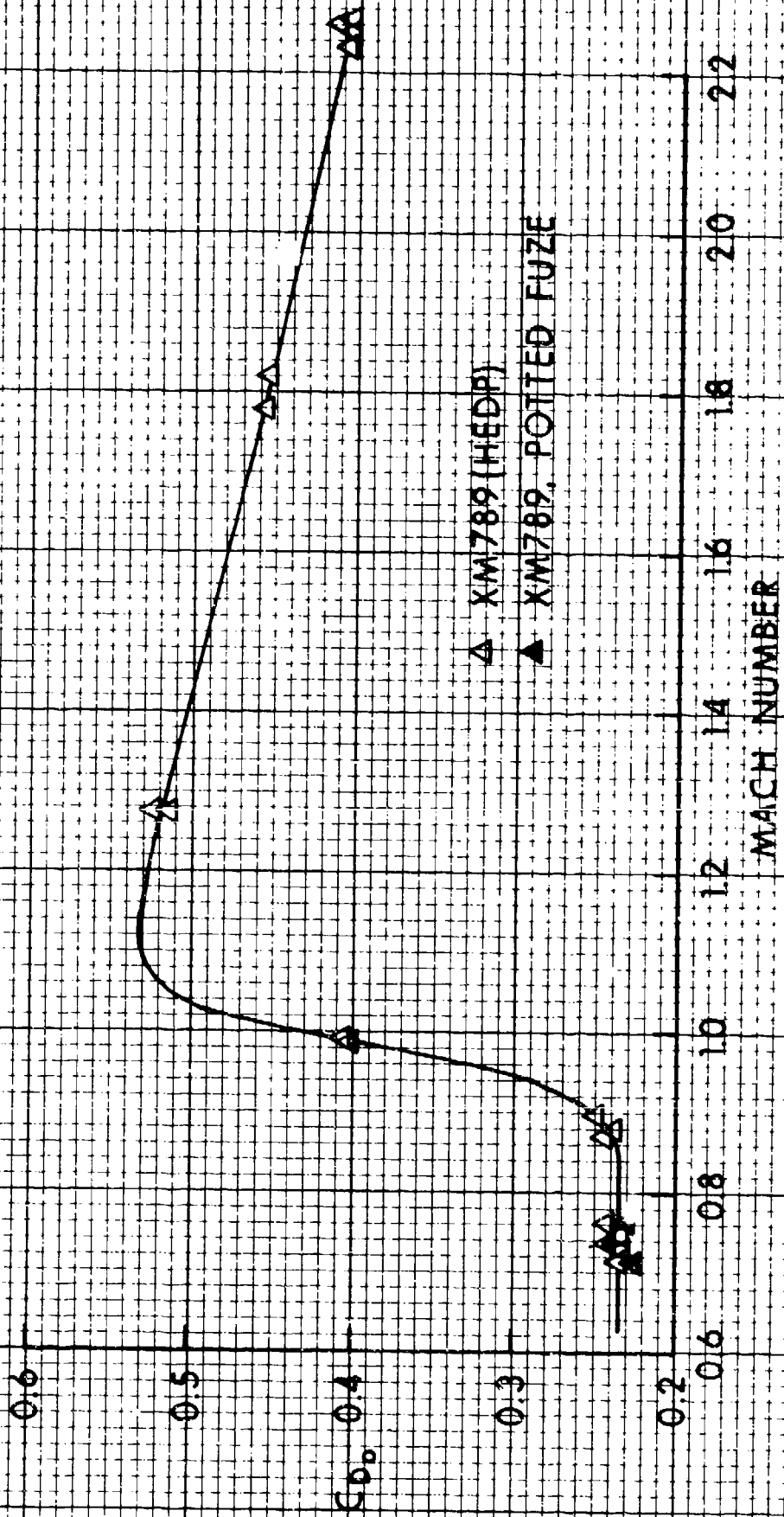
Figure 16. Zero-Yaw Drag Force Coefficient versus Mach Number, XM789

38
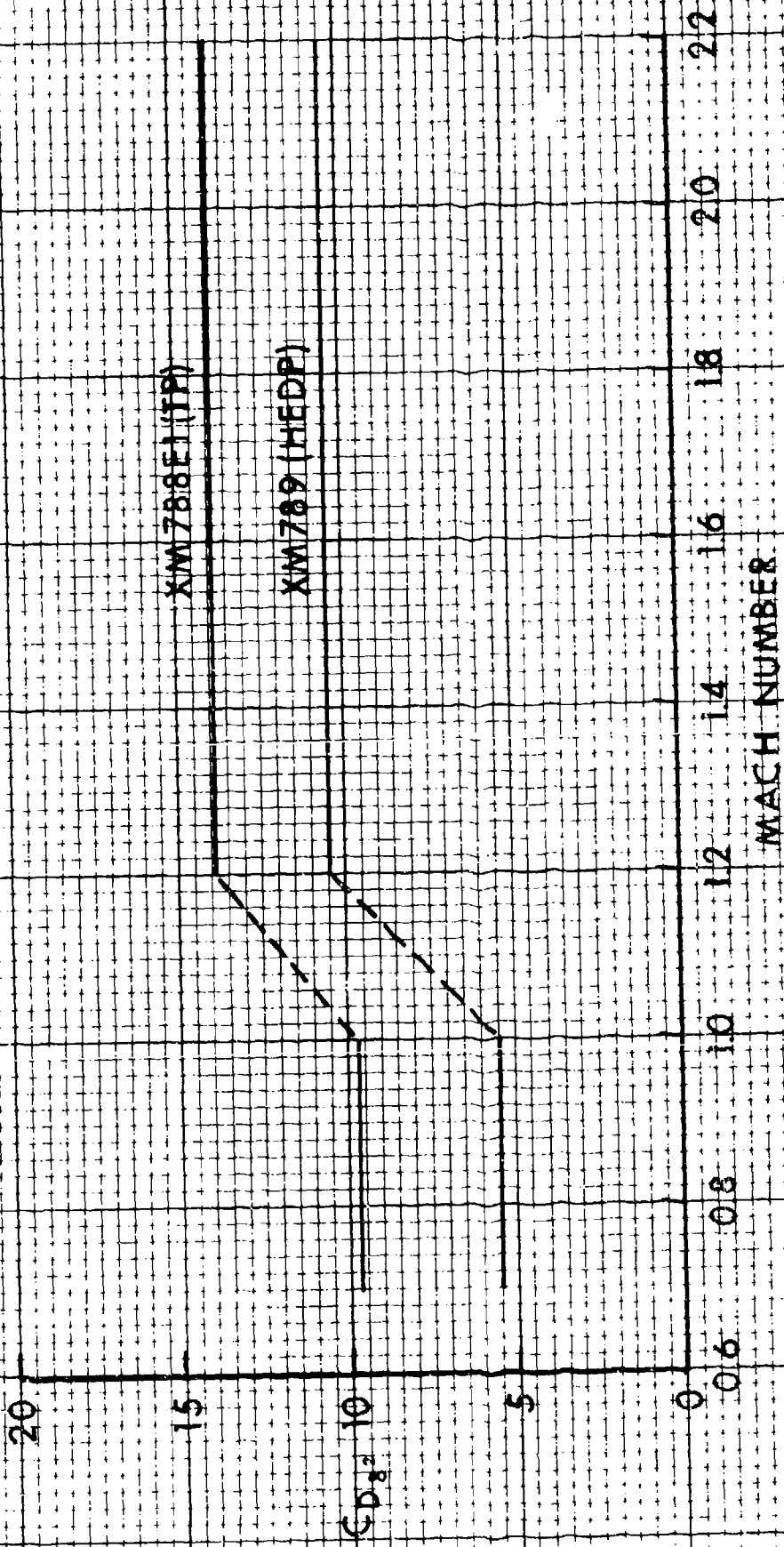
Figure 17. Yaw-Drag Force Coefficient versus Mach Number

XM788E1 (TP)

XM789 (HEDP)

$C_{D_a^2}$

MACH NUMBER

39
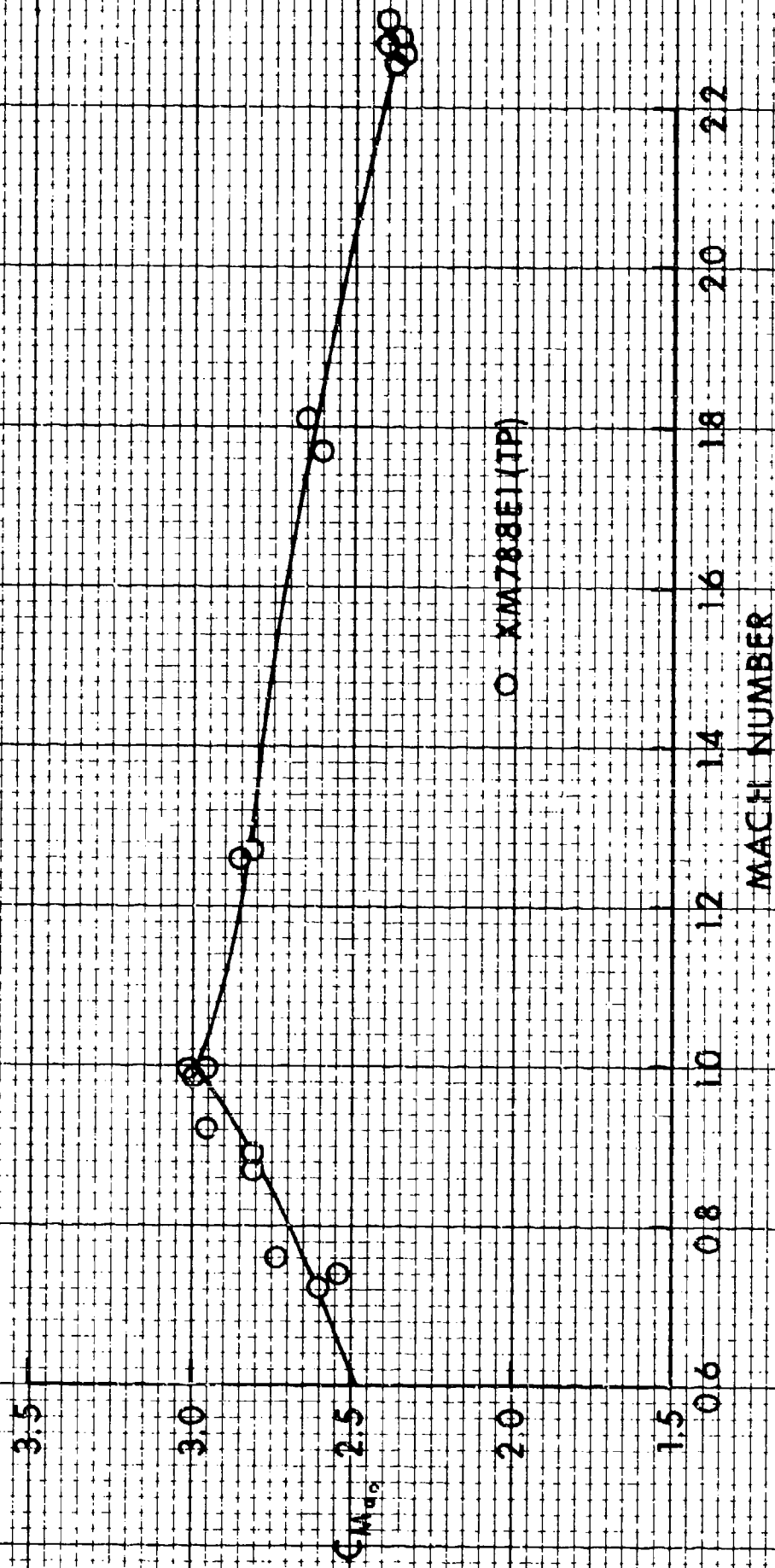
Figure 18. Zero-Yaw Pitching Moment Coefficient versus Mach Number, XM788E1

O XM788E1(TP)
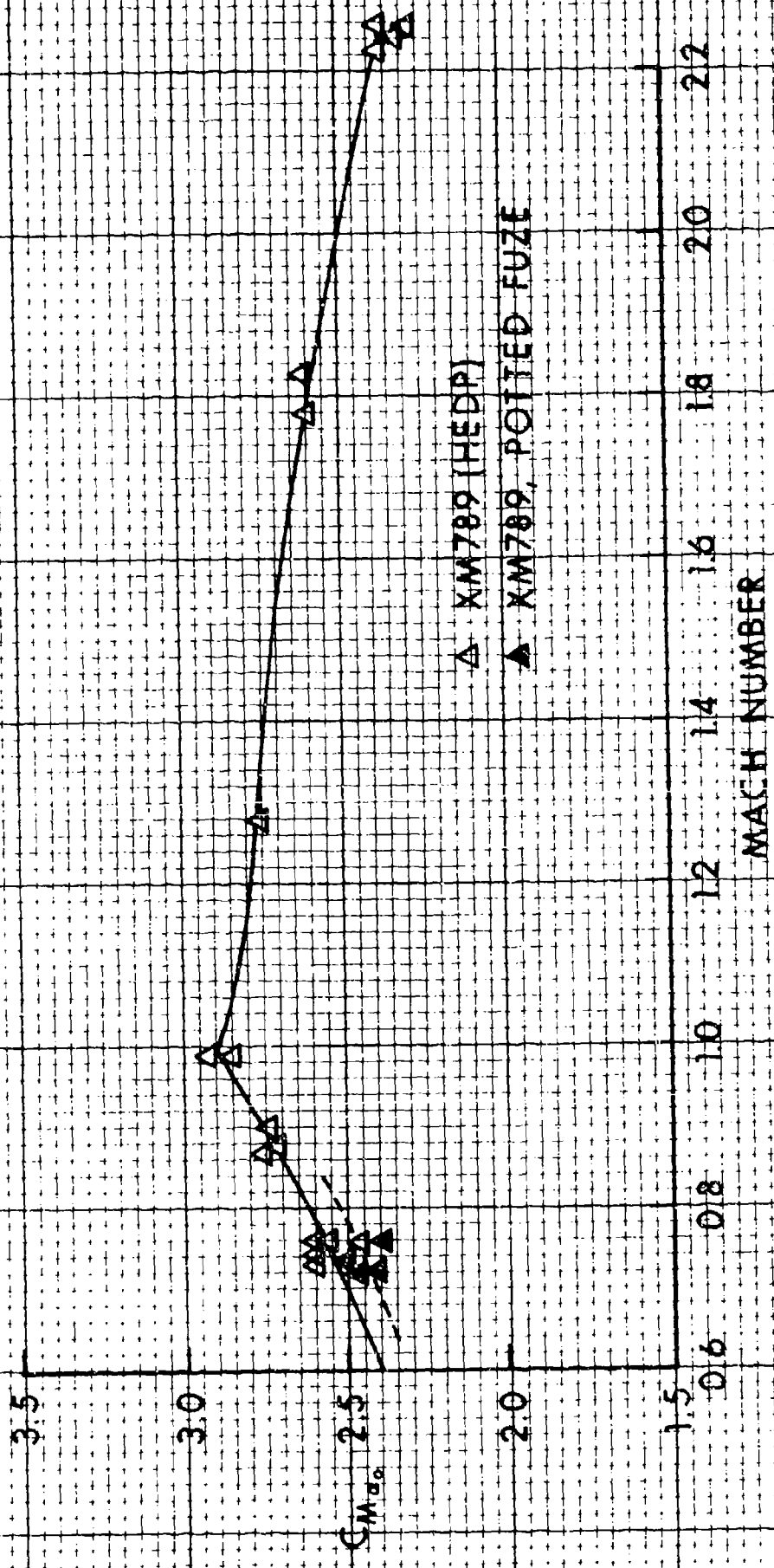
MACH NUMBER

Figure 19. Zero-Yaw Pitching Moment Coefficient versus Mach Number, XM789

41
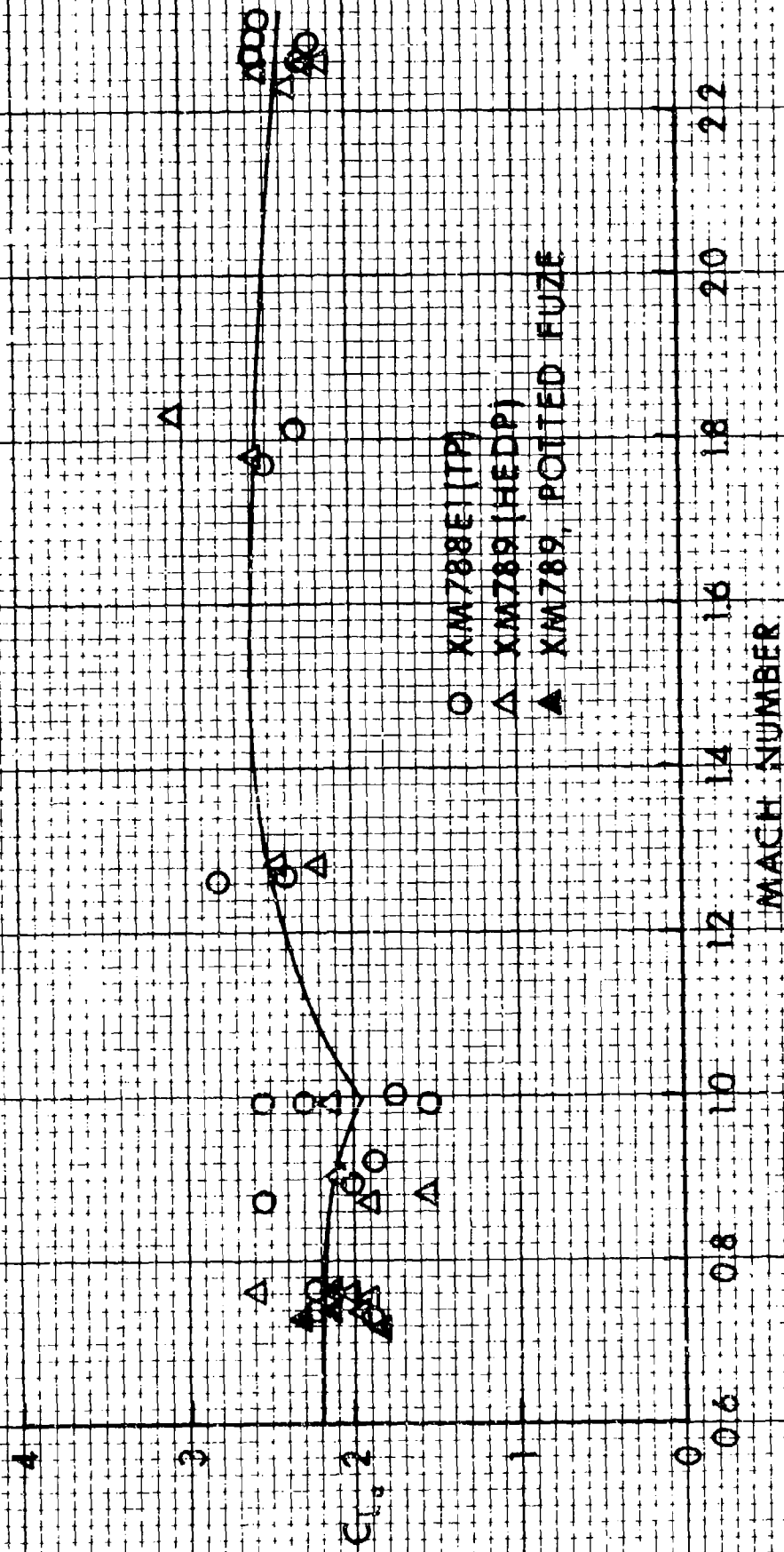
Figure 20. Lift Force Coefficient versus Mach Number

○ XM788E1(TP)
△ XM789(HEDP)
▲ XM789, POTTED FUZE

MACH NUMBER

C_{L_α}
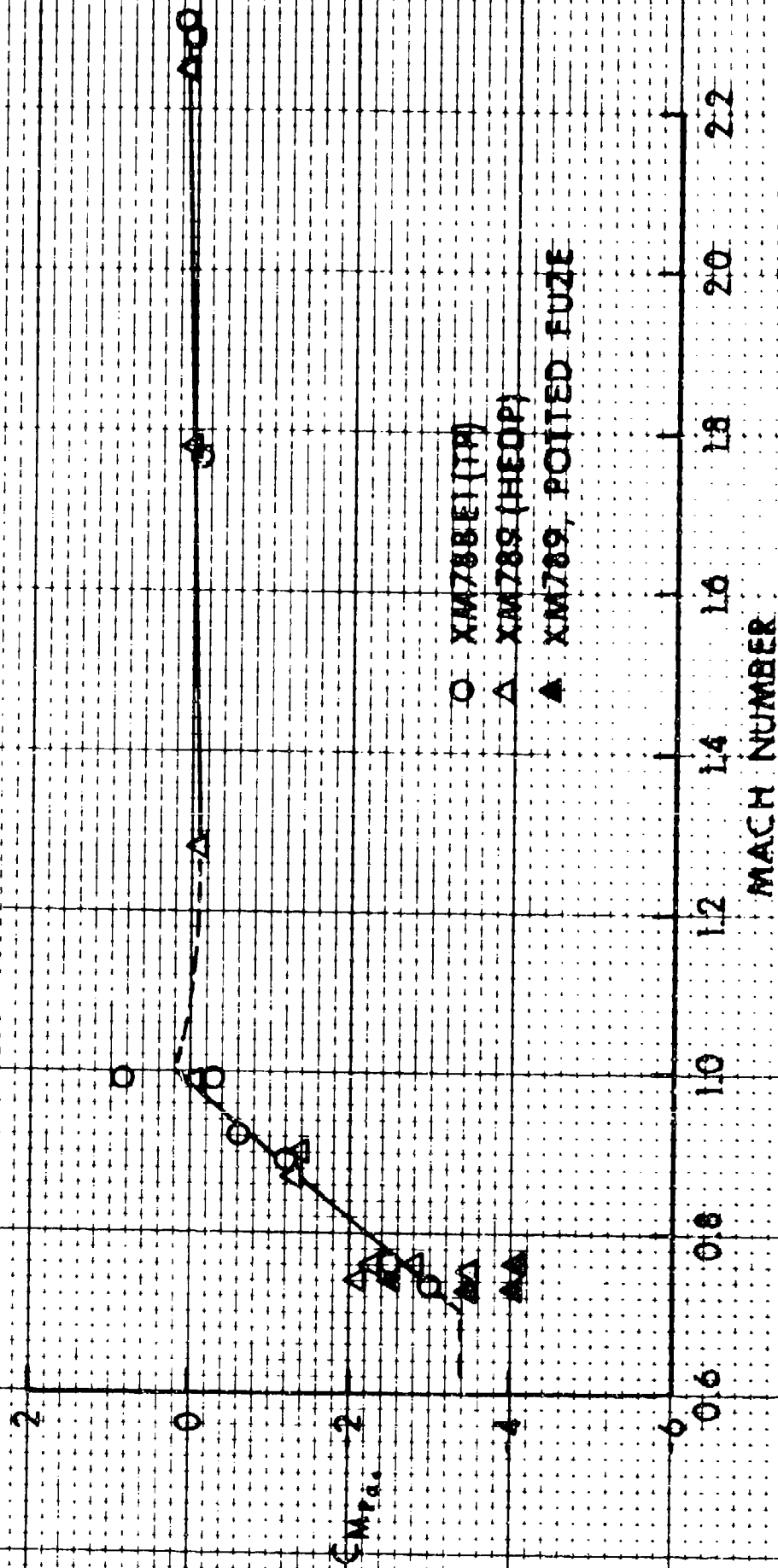
Figure 21. Zero-Yaw Magnus Moment Coefficient versus Mach Number

MACH NUMBER

$C_{M_{p\alpha}}$

O XM788E1(TP)
△ XM789 (HEDP)
▲ XM789, POINTED FUZE

43
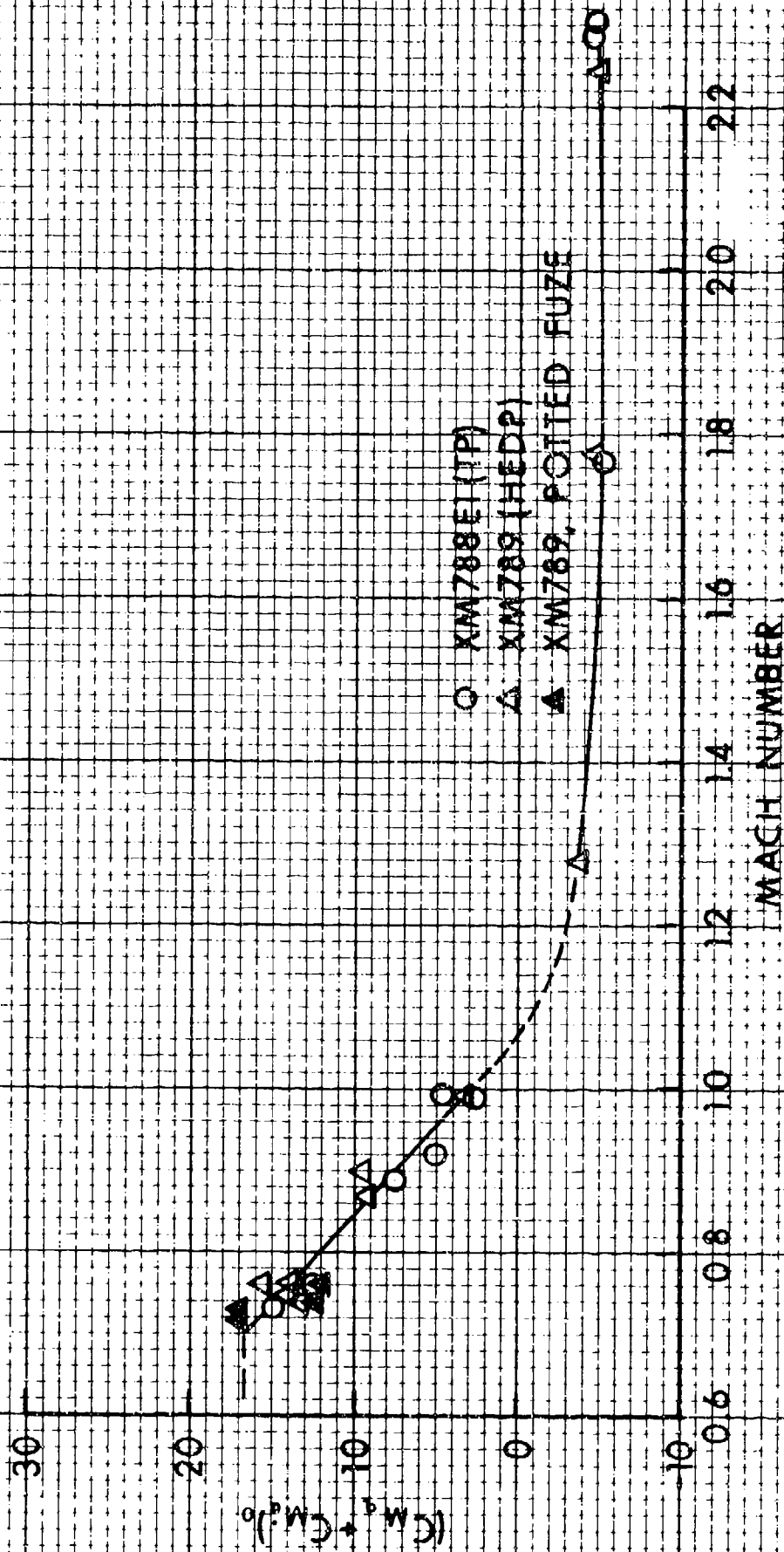
Figure 22. Zero-Yaw Pitch Damping Moment Coefficient versus Mach Number

Legend:
○ XM788EI(TP)
△ XM789 (HED2)
▲ XM789, POTTED FUZE

Y-axis: $(C_{m_q} + C_{m_{\dot\alpha}})_o$
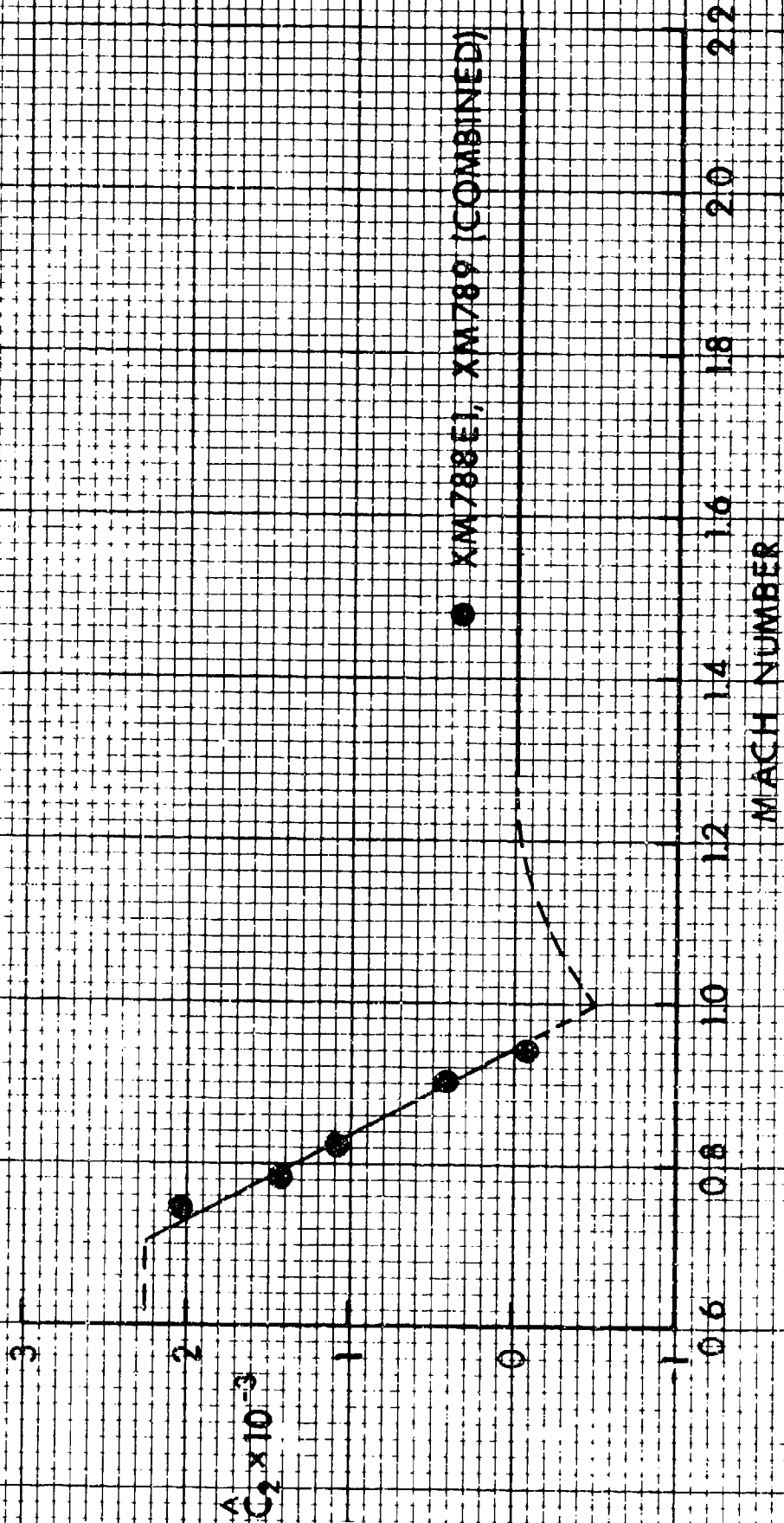
X-axis: MACH NUMBER

Figure 23. Cubic Magnus Moment Coefficient versus Mach Number

● XM788E1, XM789 (COMBINED)

MACH NUMBER

$\hat{C}_2 \times 10^{-3}$
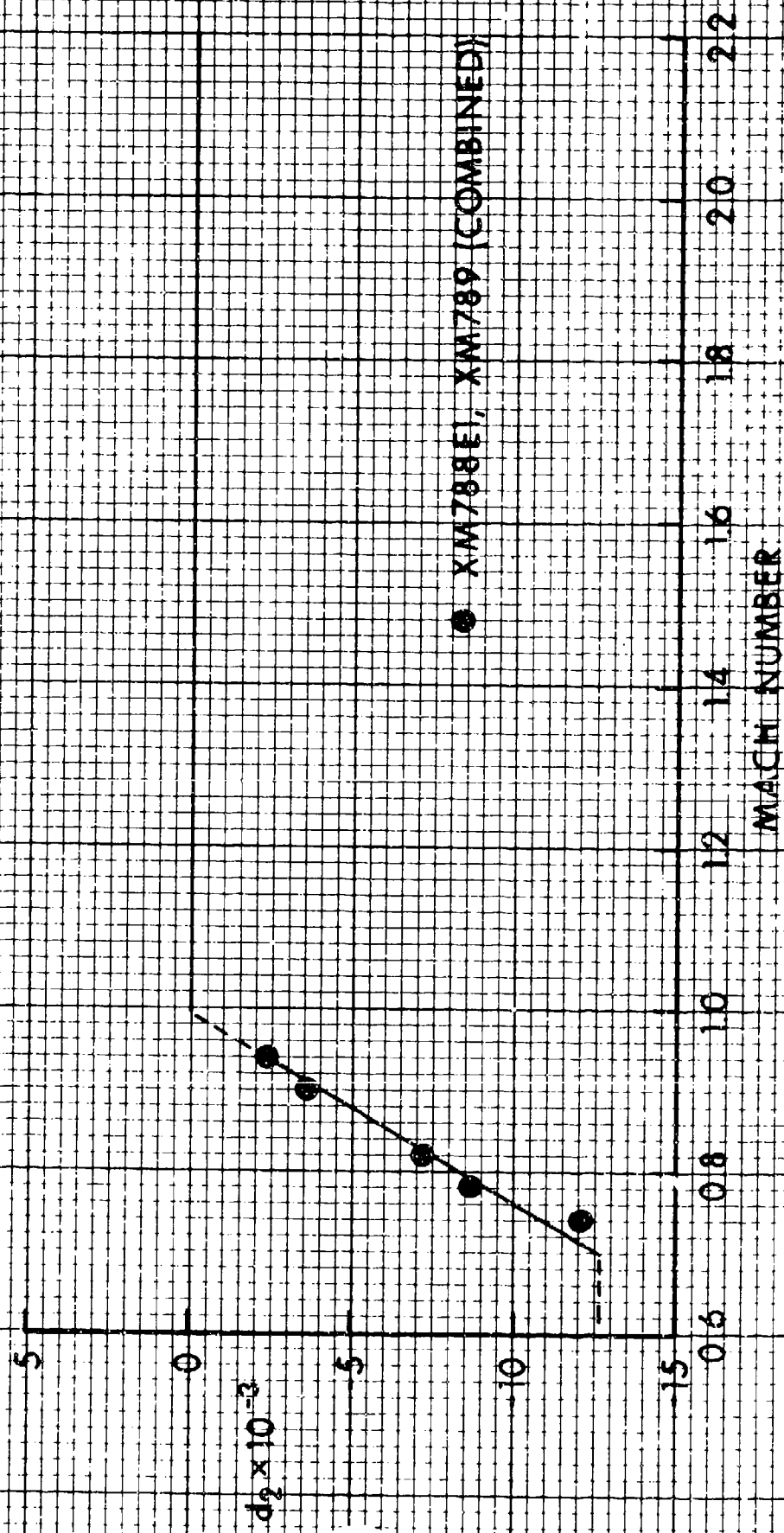
Figure 24. Cubic Pitch Damping Moment Coefficient versus Mach Number

● XM788E1, XM789 (COMBINED)

MACH NUMBER

$d_2 \times 10^{-3}$
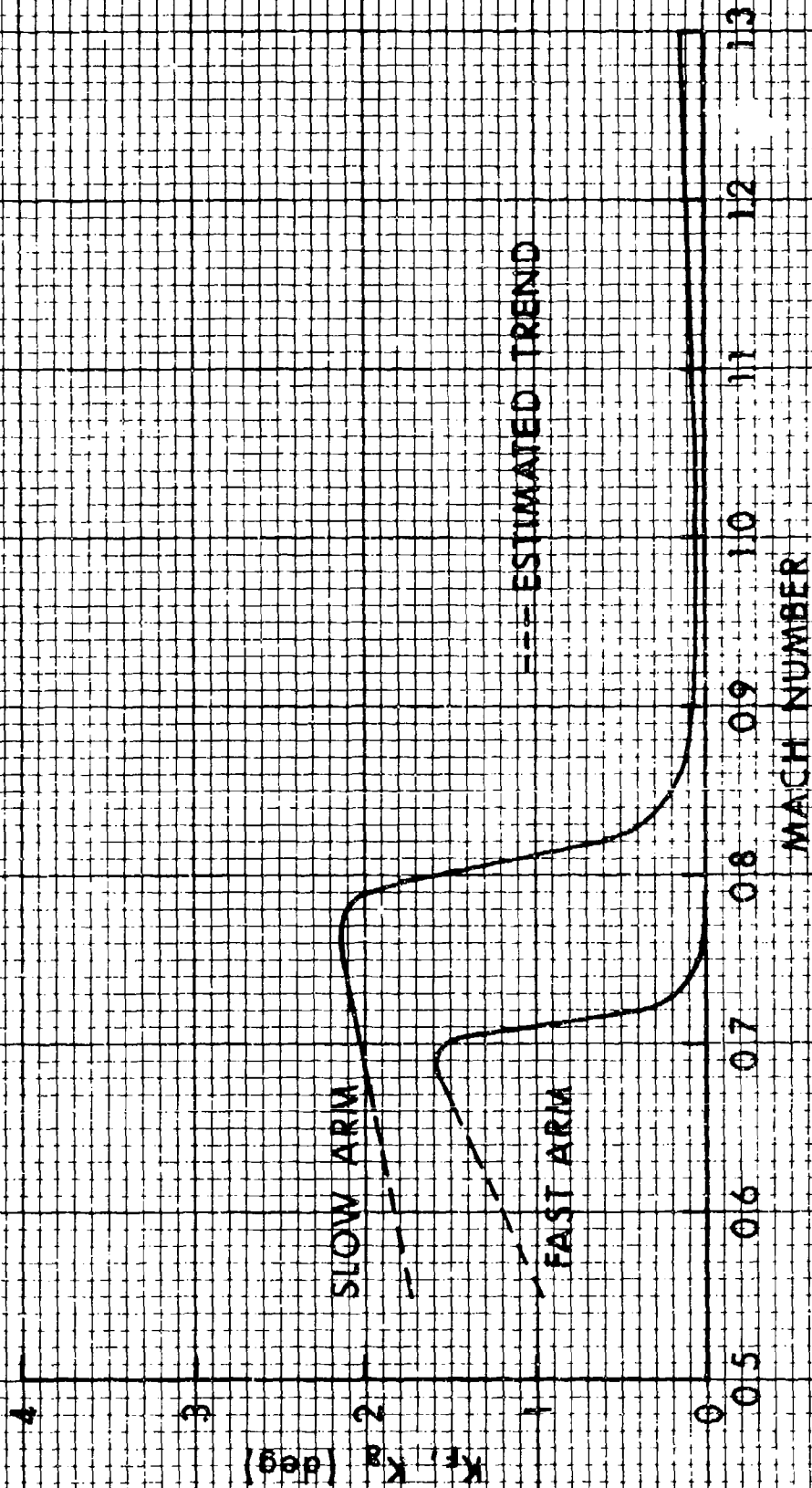
Figure 25. Fast and Slow Arm Amplitudes versus Mach Number, XM789

47
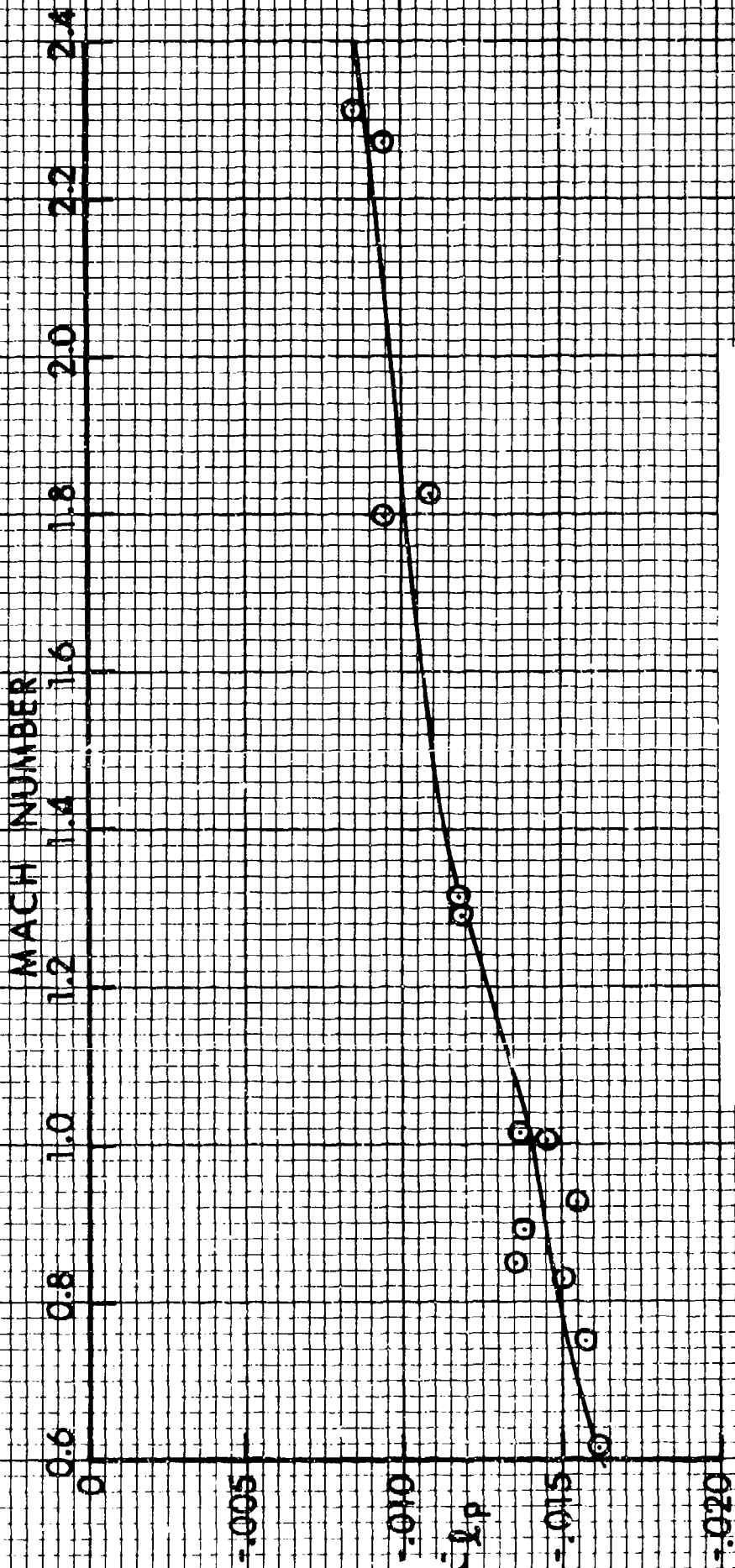
Figure 26.   Spin Damping Moment Coefficient versus Mach Number, XM788

REFERENCES

1. R. L. McCoy, "Aerodynamic Characteristics of the 30mm XM788 Projectile," Ballistic Research Laboratory Memorandum Report ARBRL-MR-03019, May 1980. AD A086096.

2. C. H. Murphy, "Data Reduction for the Free Flight Spark Ranges," Ballistic Research Laboratories Report No. 900, February 1954. AD 35833.

3. C. H. Murphy, "The Measurement of Non-Linear Forces and Moments by Means of Free Flight Tests," Ballistic Research Laboratories Report No. 974, February 1956. AD 93521.

4. C. H. Murphy, "Free Flight Motion of Symmetric Missiles," Ballistic Research Laboratories Report No. 1216, July 1963. AD 442757.

5. R. F. Lieske and R. L. McCoy, "Equations of Motion of a Rigid Projectile," Ballistic Research Laboratories Report No. 1244, March 1964. AD 441598.

a_2 = cubic lift force coefficient

C_2 = cubic static moment coefficient

$\hat{C}_2$ = cubic Magnus moment coefficient

C_D = $\dfrac{\text{Drag Force}}{(1/2)\ \rho\ V^2\ S}$

C_{D_0} = zero yaw drag coefficient

$C_{D_{\delta^2}}$ = quadratic yaw drag coefficient

C_{L_α} = $\dfrac{\text{Lift Force}}{(1/2)\ \rho\ V^2\ S\ \delta}$ Positive coefficient: Force in plane of total angle of attack, α_t, $\perp$ to trajectory in direction of α_t. (α_t directed from trajectory to missile axis.) $\delta = \sin \alpha_t$.

C_{N_α} = $\dfrac{\text{Normal Force}}{(1/2)\ \rho\ V^2\ S\ \delta}$ Positive coefficient: Force in plane of total angle of attack, α_t, $\perp$ to missile axis in direction of α_t.

$$C_{N_\alpha} \cong C_{L_\alpha} + C_D$$

C_{M_α} = $\dfrac{\text{Static Moment}}{(1/2)\ \rho\ V^2\ S\ d\ \delta}$ Positive coefficient: Moment increases angle of attack α_t.

$C_{M_{p\alpha}}$ = $\dfrac{\text{Magnus Moment}}{(1/2)\ \rho\ V^2\ S\ d\ \left(\frac{pd}{V}\right)\ \delta}$ Positive coefficient: Moment rotates nose $\perp$ to plane of α_t in direction of spin.

$C_{N_{p\alpha}}$ = $\dfrac{\text{Magnus Force}}{(1/2)\ \rho\ V^2\ S\ \left(\frac{pd}{V}\right)\ \delta}$ Negative coefficient: Force acts in direction of 90° rotation of the positive lift force against spin.

51

For most exterior ballistic uses, where $\dot{\alpha} = q$, $\dot{\beta} = -r$, the definition of the damping moment sum is equivalent to:

$C_{M_q} \quad C_{M_\alpha}$ $= \dfrac{\text{Damping Moment}}{(1/2) \quad V^2 \; S \; d \left(\dfrac{q_t d}{V}\right)}$ Positive coefficient: Moment increases angular velocity.

C_{ℓ_p} $= \dfrac{\text{Roll Damping Moment}}{(1/2) \; \rho \; V^2 \; S \; d \left(\dfrac{pd}{V}\right)}$ Negative coefficient: Moment decreases rotational velocity.

CP_N $=$ center of pressure of the normal force, positive from base to nose

α, β $=$ angle of attack, side slip

α_t $= (\alpha^2 + \beta^2)^{1/2} = \sin^{-1} \delta$, total angle of attack

λ_F $=$ fast mode damping rate

negative λ indicates damping

λ_S $=$ slow mode damping rate

ρ $=$ air density

ϕ'_F $=$ fast mode frequency

ϕ'_S $=$ slow mode frequency

c.m. $=$ center of mass

d $=$ body diameter of projectile, reference length

d_2 $=$ cubic pitch damping moment coefficient

I_x $=$ axial moment of inertia

I_y = transverse moment of inertia

K_F = magnitude of the fast yaw mode

K_S = magnitude of the slow yaw mode

ℓ = length of projectile

m   = mass of projectile

M   = Mach number

p   = roll rate

q, r   = transverse angular velocities

q_t = $(q^2 + r^2)^{1/2}$

R   = subscript denotes range value

s   = dimensionless arc length along the trajectory

S   = $\frac{\pi \, d^2}{4}$, reference area

S_d = dynamic stability factor

S_g = gyroscopic stability factor

V   = velocity of projectile

V_{Muzzle} = launch velocity of projectile

$V_{A/C}$ = aircraft velocity

Effective Squared Yaw Parameters

$$\tilde{\delta} \quad \cong \quad K_F{}^2 + K_S{}^2$$

$$\delta_e{}^2 \quad = \quad K_F{}^2 + K_S{}^2 + \frac{\phi_F' \, K_F{}^2 - \phi_S' \, K_S{}^2}{\phi_F' - \phi_S'}$$

$$\delta_{eF}{}^2 \quad = \quad K_F{}^2 + 2K_S{}^2$$

$$\delta_{eS}{}^2 \quad = \quad 2K_F{}^2 + K_S{}^2$$

$$\delta_{eHT}{}^2 \quad = \quad \left(\frac{I_Y}{I_X}\right) \frac{\left(\phi'_F + \phi'_S\right)\left(K_S{}^2 - K_F{}^2\right)}{\left(\phi_F' - \phi_S'\right)}$$

$$\delta_{eTH}{}^2 \quad = \quad \left(\frac{I_X}{I_Y}\right) \frac{\left(K_F{}^2 \, \phi_F'{}^2 - K_S{}^2 \, \phi_S'{}^2\right)}{\left(\phi_F'{}^2 - \phi_S'{}^2\right)}$$

$$\delta_{eHH}{}^2 \quad = \quad \frac{\left(\phi_F' \, K_S{}^2 - \phi_S' \, K_F{}^2\right)}{\left(\phi_F' - \phi_S'\right)}$$

DISTRIBUTION LIST

No. of Copies	Organization	No. of Copies	Organization
12	Administrator Defense Technical Info Center ATTN: DTIC-DDA Cameron Station Alexandria, VA 22314	1	Commander Naval Air Systems Command ATTN: Code AIR54112F Mr. J. Ramnarace Washington, DC 20360

1	Commander
	US Army Materiel Development
	  and Readiness Command
	ATTN: DRCDMD-ST
	5001 Eisenhower Avenue
	Alexandria, VA 22333
		1	Director
			US Army Air Mobility Research
			  and Development Laboratory
			Ames Research Center
			Moffett Field, CA 94035

9	Commander
	US Army Armament Research
	  and Development Command
	ATTN: DRDAR-TSS (2 cys)
	    DRDAR-LCA-FF
	      Mr. S. Wasserman
	    DRDAR-SCA-CH
	      Mr. C. Maile
	    DRDAR-SCS-E
	      Mr. J. Paz
	    DRDAR-SCF-DA
	      Mr. J. Spangler
	      Mr. W. Dziwak
	      Mr. K. Raisner
	      Mr. T. Peters
	Dover, NJ 07801
		1	Commander
			US Army Troop Support and
			  Aviation Materiel Readiness
			  Command
			ATTN: DRCPM-CO(T), Mr. M. Ryan
			P.O. Box 209
			St. Louis, MO 63166

		1	Commander US Army Communications Research and Development Command ATTN: DRDCO-PPA-SA Fort Monmouth, NJ 07703

1	Commander
	US Army Armament Materiel
	  Readiness Command
	ATTN: DRSAR-LEP-L, Tech Lib
	Rock Island, IL 61299
		1	Commander
			US Army Electronics Research
			  and Development Command
			Technical Support Activity
			ATTN: DELSD-L
			Fort Monmouth, NJ 07703

1	Director US Army ARRADCOM Benet Weapons Laboratory ATTN: DRDAR-LCB-TL Watervliet, NY 12189	2	Commander US Army Missile Command ATTN: DRSMI-R DRSMI-YDL Redstone Arsenal, AL 35898

1	Commander
	US Army Aviation Research
	  and Development Command
	ATTN: DRDAV-E
	4300 Goodfellow Blvd.
	St. Louis, MO 63120
		1	Commander
			US Army Tank Automotive Research
			  and Development Command
			ATTN: DRDTA-UL
			Warren, MI 48090

		1	Commander US Army Armament Research and Development Command ATTN: DRDAR-TDC Dover, NJ 07801

DISTRIBUTION LIST (Cont)

No. of Copies	Organization
2	Program Manager Advanced Attack Helicopter, DARCOM ATTN: DRCPM-AAH-PM, Mr.J. Romano Mr. A. Corgiat 4300 Goodfellow Blvd. St. Louis, MO 63120
1	Director US Army TRADCOC Systems Analysis Activity ATTN: ATAA-SL, Tech Lib White Sands Missile Range NM 88002
4	AFATL/DLDL ATTN: G. Winchenbach K. West K. Cobb Tech Lib Eglin AFB, FL 32542
1	General Electric Company Armaments Systems Dept. ATTN: Mr. R.H. Whyte Lakeside Avenue Burlington, VT 05401
1	Honeywell, Inc. Govt & Aerospace Products Div ATTN: Mr. Millivolte 600 Second Street, NE Hopkins, MN 55343
1	Honeywell, Inc. Defense Systems Division ATTN: Mr. G. Stilley 5901 S. County Road 18 Ediva, MN 55436
1	Teledyne Systems Company Mail Stop 12 ATTN: Mr. Carl Gruvin 19601 Nordhoff St. Northridge, CA 91324

No. of Copies	Organization
1	Hughes Helicopters Advanced Attack Helicopter ATTN: Ordnance Division Mr. R. Forker Centinela and Teale Streets Culver City, CA 90230
5	Hughes Helicopters Mail Station T73A ATTN: Mr. D. Price Mr. R.J. Hopson Mr. R. Watson Mr. F. Roberts Mr. J. Smalley Building 305 2560 Walnut Avenue Culver City, CA 90230
1	Skidmore and Shean ATTN: Mr. R. Pfielsticker 1 Oxford Valley Mall Langhorne, PA 19047

Aberdeen Proving Ground

Dir, USAMSAA
ATTN: DRXSY-D
DRXSY-MP, H. Cohen
DRXSY-A, D. O'Neill
T. Coyle
C. Abel
G. Nielsen
DRXSY-G, J. Kramar
DRXSY-R, L. Gentry
DRXSY-S, R. Bailey
M. Carroll
Cdr, USATECOM
ATTN: DRSTE-TO-F
Dir, USACSL, Bldg. E3516, EA
ATTN: DRDAR-CLP-PA
Mr. M. Miller
Mr. D. Olson
Mr. J. Huerta

USER EVALUATION OF REPORT

Please take a few minutes to answer the questions below; tear out this sheet. fold as indicated, staple or tape closed, and place in the mail. Your comments will provide us with information for improving future reports.

1. BRL Report Number_____

2. Does this report satisfy a need? (Comment on purpose, related project, or other ᴜ_ᴀ of interest for which report will be used.)

_____

_____

_____

3. How, specifically, is the report being used? (Information source, design data or procedure, management procedure, source of ideas, etc.)_____

_____

_____

4. Has the information in this report led to any quantitative savings as far as man-hours/contract dollars saved, operating costs avoided, efficiencies achieved, etc.? If so, please elaborate.

_____

_____

5. General Comments (Indicate what you think should be changed to make this report and future reports of this type more responsive to your needs, more usable, improve readability, etc.)_____

_____

_____

_____

6. If you would like to be contacted by the personnel who prepared this report to raise specific questions or discuss the topic, please fill in the following information.

                    Name:_____

           Telephone Number:_____

Organization Address:_____

_____

_____